



Enhanced dataset of global marine isoprene emission from biogenic and photochemical processes for the period 2001-2020

Lehui Cui¹, Yunting Xiao¹, Wei Hu¹, Lei Song², Yujue Wang³, Chao Zhang³, Pingqing Fu¹, Jialei Zhu¹

¹Institute of Surface-Earth System Science, School of Earth System Science, Tianjin University, Tianjin, 300072, China

5 ²Center for Monsoon System Research, Institute of Atmospheric Physics, Chinese Academy of Sciences, Beijing, 100029, China

³Frontiers Science Center for Deep Ocean Multispheres and Earth System, and Key Laboratory of Marine Environment and Ecology, Ministry of Education, Ocean University of China, Qingdao 266100, China

Correspondence to: J. Zhu (zhujialei@tju.edu.cn)

10 **Abstract.** Isoprene is a crucial non-methane biogenic volatile organic compound (BVOC) that exhibits the largest emissions globally. It is chemically reactive in the atmosphere and serves as the primary source to generate of secondary organic aerosols (SOA) in terrestrial and remote marine regions. However, a comprehensive estimation of marine isoprene emissions is currently lacking. Here we built a module to present a twenty-year (2001-2020) global hourly dataset for marine isoprene emissions, including phytoplankton-generated biological emissions (BIO emissions) and photochemistry-generated emissions in the sea surface microlayer (SML emissions) based on the latest advancements in biological, physical, and chemical processes, with high spatial and temporal resolutions. The ERA5-hourly meteorological reanalysis ($0.25^\circ \times 0.25^\circ$ horizontal spatial resolution) from the European Centre for Medium-Range Weather Forecasts (ECMWF) for the period of 2001-2020 were used as input for meteorological factors. Chlorophyll concentration data and the downwelling radiative flux diffuse attenuation coefficient data were collected from the National Aeronautics and Space Administration's (NASA) Ocean Color Web MODIS Level-3 data, with a resolution of 9 km, covering the same period. Additionally, monthly normalized water-leaving radiance at 410 nm data from the Visible and Infrared Imager/Radiometer Suite (VIIRS) were provided by the National Oceanic and Atmospheric Administration (NOAA). Our dataset suggests the annual global marine isoprene emissions amount to $1.049 \pm 0.009 \text{ Tg}\cdot\text{yr}^{-1}$. Among these, the BIO emissions are $0.433 \pm$
15 $0.007 \text{ Tg}\cdot\text{yr}^{-1}$ while SML emissions contribute $0.616 \pm 0.003 \text{ Tg}\cdot\text{yr}^{-1}$. The ability of this module to estimate marine isoprene emissions was evaluated through comparison with a series of observations of marine isoprene concentrations and emission fluxes. Annual total isoprene emission across tropical ocean shows a declining trend from 2001 to 2020. Most ocean regions exhibit a one-year emission period, whereas a significant intraseasonal period is found in the tropical ocean. This dataset can be employed as input for the simulation of marine SOA
20 formation in earth system models. This work provides the foundation for further studies into the impact of the air-
30



sea system on marine SOA formation and its climate effect. The DOI link for the dataset is <http://dx.doi.org/10.11888/Atmos.tpdc.300521> (Cui and Zhu., 2023).

1 Introduction

Biogenic organic volatile compounds (BVOCs), one of the most important components in the marine boundary layer (MBL), serves as an important role in marine secondary organic aerosols (SOAs) formation, particularly in pristine remote ocean (Yu and Li, 2021). Once the BVOCs are emitted into the marine boundary layer, they will be oxidized by hydroxyl radicals, ozone or other radicals, resulting in the formation of low-volatility oxides. These oxides have the potential to undergo subsequent transformations leading to the production of SOAs (Meskhidze et al., 2011; Gantt et al., 2012; Claeys et al., 2004). Due to their typical short lifetime in the atmosphere, it is difficult for most BVOCs emitted from terrestrial sources to undergo long-range transport. As a result, marine BVOC emissions likely exert a dominant influence on BVOC concentrations over the remote ocean (Dani and Loreto, 2017; Guenther et al., 2006; Kameyama et al., 2014). SOA generated from BVOCs has a large effect on the radiation budget and cloud microphysical properties, thereby exerting a substantial influence on global climate change (Rosenfeld et al., 2014; Gantt et al., 2012).

Among all the non-methane BVOCs species, isoprene exhibits a large emission and demonstrates significant atmospheric chemical reactivity in the marine environment (Yokouchi et al., 1999; Guenther et al., 2012; Novak and Bertram, 2020). Previous studies have estimated marine isoprene emissions using both bottom-up and top-down approaches. Bottom-up methods yielded emission estimates in the range of 0.11-1.36 Tg·yr⁻¹ (Gantt et al., 2009; Arnold et al., 2009; Booge et al., 2016; Conte et al., 2020; Myriokefalitakis et al., 2010; Palmer and Shaw, 2005; Sinha et al., 2007; Luo and Yu, 2010; Kim et al., 2017; Brüggemann et al., 2018; Shaw et al., 2010), while top-down methods yielded estimates in the range of 1.90-13.15 Tg·yr⁻¹ (Luo and Yu, 2010; Arnold et al., 2009). Over the past decades, numerous studies have provided estimates of BIO emissions and SML emissions over the global ocean. The estimation of BIO emissions is typically derived from an empirical linear relationship established between ocean chlorophyll concentration and isoprene emissions. (Palmer and Shaw, 2005). This is because isoprene is a structural component and metabolic degradation product of various plant photosynthetic pigments such as chlorophyll and carotenoids (Hackenberg et al., 2017; Dani and Loreto, 2017; Booge et al., 2016). The empirical linear relationship can be further refined by taking into account different types of phytoplankton, which can vary in terms of their photosynthetic pigments and metabolic processes (Arnold et al., 2009; Gantt et al., 2009). Several enhancements and refinements have been incorporated into the calculation of BIO emissions. These



60 updates include the dynamic euphotic zone (Gantt et al., 2009) and observation-based biochemical loss (Shaw et al., 2003; Simo et al., 2022).

The estimation of SML emissions is based on the surfactants present in the sea surface microlayer and their associated photochemical processes (Brüggemann et al., 2018; Conte et al., 2020). The sea surface microlayer (SML) acts as a flimsy interfacial layer between the marine atmosphere and the ocean. It is formed by natural
65 surfactants produced through phytoplankton and other marine biological processes (Wurl et al., 2011). In previous studies, the quantification of surfactant enrichment in the SML was determined using net primary production (NPP), which serves as an indicator of phytoplankton productivity. Previous studies utilized experimentally based parameters to describe the photochemical processes within the SML, as well as a 10-metre windspeed threshold indicating the point at which the SML starts to be torn apart (Ciuraru et al., 2015b; Brüggemann et al., 2017). To
70 date, estimates of global marine isoprene emissions have been derived by considering these two emission pathways (Conte et al., 2020; Zhang and Gu, 2022). However, few long-term datasets with high temporal and spatial resolutions is available for both types of emission till now. Previous estimates also encountered challenges related to data availability and unclear emission mechanisms, leading to uncertainties in the estimated emissions. Estimations for high latitudes are particularly lacking due to limited satellite data coverage during the winter months.
75 Moreover, previous estimations of vertical distributions of chlorophyll and isoprene concentrations did not entirely align with current observed vertical profiles in the subsurface ocean (Conte et al., 2020; Gantt et al., 2009; Zhang and Gu, 2022). The relationships between emissions and marine and meteorological factors, established based on localized phytoplankton populations, are regionally constrained and may not be applicable in all situations. These limitations led to discrepancies between observed emissions and the estimations obtained using previous methods.
80 Isoprene exhibits a lifetime of approximately 10-100 days in seawater (Booge et al., 2018). Once released into the atmosphere, it rapidly reacts with OH radicals, resulting in a short atmospheric lifetime of about one hour (Kameyama et al., 2014). Within the marine boundary layer (MBL), isoprene can undergo oxidation, leading to the formation of semi-volatile organic compounds (SVOCs) and low-volatility organic compounds (LVOCs) such as methacrolein and methacrylic acid. These compounds actively participate in the generation of marine secondary
85 organic aerosols (SOAs) (Claeys et al., 2004; Kim et al., 2017). Due to its significant emissions and capacity to contribute to SOA formation, marine isoprene plays a crucial role in aerosol generation and growth within the MBL. The estimation of marine isoprene emission is essential and serves as a fundamental aspect for future studies on marine SOAs and their climate effects (Carslaw et al., 2010).

Here, we generated a $0.25^{\circ} \times 0.25^{\circ}$ grid dataset of global marine isoprene emissions covering a twenty-year period
90 from 2001 to 2020 with an updated method combining the latest emission features and state-of-the-art influencing



factors. Two distinct types of emissions are separately calculated by satellite-derived monthly ocean chlorophyll concentration data from MODIS and hourly reanalysis meteorological data from ECMWF. Our dataset can be used as input data for climate or atmospheric chemistry models within the marine domain. The module also can be coupled with the earth system model to calculate marine isoprene emissions online.

95 The subsequent section (Sect. 2) elucidates the data, methods and factors employed in our estimation of marine isoprene emissions. Our results are compared with previous isoprene emission inventories and some field observations in Sect. 3. Sect. 4 provides information on our dataset and data availability. The characteristics of the marine isoprene emission are analysed in the Sect. 5. Sect. 6 is the conclusions and discussions.

2 Methods

100 2.1 Input data

Twenty years (2001-2020) monthly average chlorophyll concentration data at 9 km resolution and downwelling radiative flux diffuse attenuation coefficient data were obtained from MODIS Level 3 product in the National Aeronautics and Space Administration (NASA)'s Ocean Color Web (<https://oceancolor.gsfc.nasa.gov>). These two datasets were averaged into grids with a resolution of $0.25^{\circ} \times 0.25^{\circ}$ to fit the fifth generation European Centre for
105 Medium-Range Weather Forecasts (ECMWF) atmospheric reanalysis (ERA5) dataset used in this study (Hersbach et al., 2023). The hourly average 10-metre u-wind and v-wind component, 2-metre temperature, sea surface temperature and surface downwelling shortwave flux were applied in the module. Additionally, the monthly normalized water-leaving radiance at 410 nm for 2012-2020 from the National Oceanic and Atmospheric Administration (NOAA) (<https://coastwatch.noaa.gov>) were utilized to determine the distribution of phytoplankton
110 types together with chlorophyll concentration. The most prevalent phytoplankton types on a monthly basis from 2012 to 2020 were determined for estimations of isoprene emissions over the twenty-year period.

2.2 The BIO emission module

The phytoplankton-generated emission module was developed based on the assumption that the concentration of isoprene in the ocean remains static. This assumption implies that the net isoprene production, accounting for
115 biochemical costs, is approximately equal to the isoprene flux from the ocean to the MBL. Since isoprene will be oxidized immediately once it enters the MBL because of its high chemical reactivity, the model assumes that the isoprene mixing ratio in the MBL is negligible. The BIO model can be expressed by the following equations:

$$F_b = \alpha \cdot P \cdot S, \quad (1)$$



where F_b ($\text{g} \cdot \text{grid}^{-1} \cdot \text{h}^{-1}$) represents the isoprene emission flux from the air-sea interface into the MBL, P ($\text{g} \cdot \text{m}^{-2} \cdot \text{h}^{-1}$) is the isoprene production rate generated by phytoplankton, S (m^2) is the grid cell area and α is a chlorophyll-based dimensionless factor to determine the biochemical costs of isoprene in seawater. The value of α is calculated by the following equation based on previous observational study (Simo et al., 2022):

$$\alpha = 0.14 \times C_{chl}^{1.28} + 0.05 \quad (\text{When } C_{chl} < 5.77 \text{ mg m}^{-3})$$
$$\alpha = 0.373 \quad (\text{When } C_{chl} \geq 5.77 \text{ mg m}^{-3}). \quad (2)$$

The term $0.14 \times C_{chl}^{1.28}$ represents the degradation and utilization of isoprene by heterotrophic bacteria. It accounts for the observed correlation between higher bacterial activity and higher chlorophyll concentrations in the mixed layer. The second term of 0.05 represents empirical chemical loss of isoprene (Palmer and Shaw, 2005; Booge et al., 2018). It is important to note that when the seawater chlorophyll concentration exceeds $5.77 \text{ mg} \cdot \text{m}^{-3}$, α is set to a constant value of 0.373 to ensure a maximum stable biochemical loss term. This approach is based on observations where the maximum seawater chlorophyll concentration was observed at $5.77 \text{ mg} \cdot \text{m}^{-3}$ (Simo et al., 2022). Therefore, the specific value of 0.373 was determined to account for biochemical loss in nutrient-rich environments.

The isoprene production rate P , is determined through the application of a linear relationship between chlorophyll concentration, radiation, and the diffuse attenuation coefficient at 490 nm, as well as the classification of phytoplankton types. Four distinct types of phytoplankton (i.e. haptophytes, *Prochlorococcus*, *Synechococcus*-like cyanobacteria and diatoms) are involved, each with a different isoprene production rate defined below. A comprehensive explanation of the methodology used to identify the phytoplankton types will be provided in Sect. 2.3.

Here, the Eq. (3) is for isoprene production rate:

$$P = I \cdot C_{chl} \cdot T_c. \quad (3)$$

In the Eq. (3), T_c ($\mu\text{mol isoprene} \cdot (\text{g chl a})^{-1} \cdot \text{h}^{-1}$) is a coefficient that accounts for the different abilities of phytoplankton types to produce isoprene. These coefficients were determined in previous studies, which will be discussed in the next section. C_{chl} ($\text{mg} \cdot \text{m}^{-3}$) represents the sea surface chlorophyll concentration, which is considered as a parameter within the mixed layer of each grid cell. I (m) is the integrated result of radiation in the planktonic euphotic zone, where:

$$I = 2 \ln\left(\frac{2I_0}{3600}\right) H_{max} - k_{490} \cdot H_{max}^2. \quad (4)$$



I is limited by the maximum depth H_{max} (m) (Gantt et al., 2009; Shaw et al., 2003), which is calculated by:

$$H_{max} = \left(-\ln\left(\frac{I}{I_0}\right) \cdot k_{490}^{-1}\right). \quad (5)$$

In Eq. (4)&(5), k_{490} (m^{-1}) is the diffuse attenuation coefficient of downwelling radiative flux at 490 nm, which
 150 characterize the downwelling irradiance within the water column. Finally, I_0 ($\text{J}\cdot\text{m}^{-2}$) is surface solar downward
 radiation, for which we used hourly data here.

The aforementioned equations were utilized to estimate the hourly marine isoprene emissions originating from
 phytoplankton within each grid, with a spatial resolution of $0.25^\circ \times 0.25^\circ$. The diurnal variation of isoprene BIO
 emissions was estimated based on the hourly radiation data in this module. It should be noted that isoprene BIO
 155 emissions are negligible during night time hours due to the absence of radiation, as supported by relevant
 observational studies (Gantt et al., 2009; Sinha et al., 2007; Hackenberg et al., 2017). The mean annual BIO
 emission was calculated to be $0.433 \text{ Tg}\cdot\text{yr}^{-1}$, which is comparable to the results ($0.11\text{-}1.36 \text{ Tg}\cdot\text{yr}^{-1}$) reported by
 previous studies that employed alternative estimation methods (Table 1).

Table 1: Marine isoprene emission estimations in previous studies.

| Compounds | Emissions $\text{Tg}\cdot\text{yr}^{-1}$ | Reference |
|-----------|---------------------------------------------|----------------------------------------------------|
| Isoprene | 0.11 | (Palmer and Shaw, 2005) |
| | 1.36 | (Sinha et al., 2007) |
| | 0.79 | (Gantt et al., 2009) |
| | 0.31 | (Arnold et al., 2009) |
| | 1.90 | (Top-down) (Arnold et al., 2009) |
| | 0.99 | (Myriokefalitakis et al., 2010) |
| | 0.36 | (Luo and Yu, 2010) |
| | 13.15 | (Top-down) (Luo and Yu, 2010) |
| | 0.24 | (Booge et al., 2016) |
| | 0.65 | (Kim et al., 2017) |
| | 1.11 | (Sea Surface Microlayer) (Brüggemann et al., 2018) |
| | 0.75 | (Conte et al., 2020) |
| | 0.96 | (Li et al., 2020) |
| 1.05 | This study | |



160 2.3 Phytoplankton types distribution

Along with various oceanological conditions of different oceans on the global scale, such as temperature, salinity, nutrient and photic zone depth, dominant phytoplankton types would produce isoprene in different rate through their photosynthesis and metabolic process (Booge et al., 2018; Dani and Loreto, 2017). For instance, cyanobacteria predominantly control the isoprene emission in tropical and subtropical oceans, while diatoms exhibit higher rates at high latitudes (Dani and Loreto, 2017). Moreover, it has been observed that the larger the size of a distinct type of phytoplankton, the less likely it is to thrive in the oligotrophic region of the ocean, due to the limited specific surface area of phytoplankton cells (Alvain et al., 2008). The coefficient T_c ($\mu\text{mol isoprene} \cdot (\text{g chl}a)^{-1} \cdot \text{h}^{-1}$) in the Eq. (3), which relates chlorophyll concentration to isoprene emissions, is determined by phytoplankton type. Four types of phytoplankton and their corresponding coefficients T_c in this module are 0.028 for haptophytes, 0.029 for *Prochlorococcus*, 0.032 for *Synechococcus*-like cyanobacteria and 0.042 for diatoms (Gantt et al., 2009).

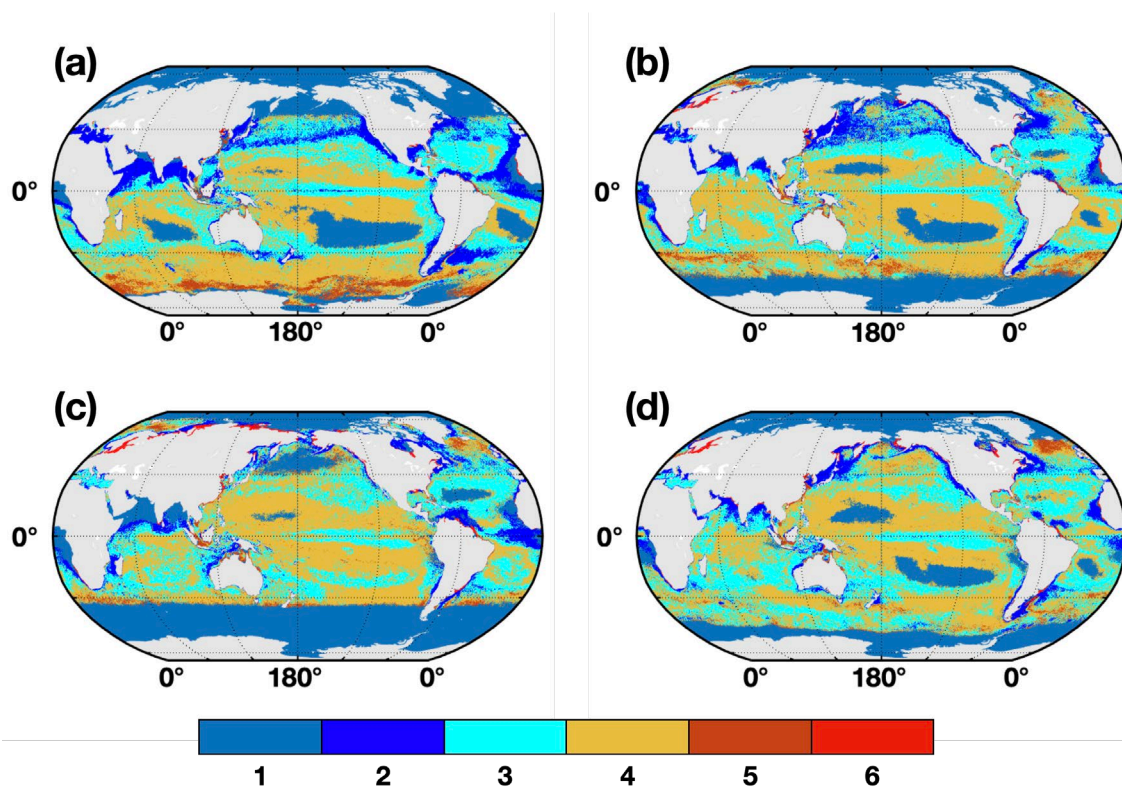
The dominant phytoplankton type was determined using monthly satellite-observed normalized water-leaving radiance at 410 nm and seawater chlorophyll concentration. This classification method is based on the distinctive effects of pigments on the normalized water-leaving radiance for each phytoplankton type (Alvain et al., 2005; Alvain et al., 2008), and the details are summarized in Table 2. A simplified scheme of normalized water-leaving radiance at 410 nm is used to determine phytoplankton types for the chlorophyll range $0.04\text{-}3 \text{ mg} \cdot \text{m}^{-3}$ (Alvain et al., 2005; Alvain et al., 2008). An “undefined type” with a coefficient of 0.028 was assigned in areas with chlorophyll concentrations below $0.04 \text{ mg} \cdot \text{m}^{-3}$, including oligotrophic regions and grids with missing values. Conversely, the chlorophyll concentration is greater than $3 \text{ mg} \cdot \text{m}^{-3}$ in many coastal areas with sufficient nutrients. The normalized water-leaving radiance data are always missing due to turbid water bodies inshore in the coastal areas, which leads to underestimated isoprene BIO emission there. Based on previous observational studies in these coastal areas, it was determined that the dominant phytoplankton type is a combination of 50 % diatoms and 50 % haptophytes in the grids with chlorophyll concentrations greater than $3 \text{ mg} \cdot \text{m}^{-3}$ (Guo et al., 2014; Li et al., 2018; Liu et al., 2016).



185 **Table 2: Scheme of phytoplankton types and classification method.**

| Chlorophyll Concentration (mg m ⁻³) | Normalized Water-leaving Radiation | Types | Factors (T_c) | |
|-------------------------------------------------|------------------------------------|-----------------------------------|------------------------------------------|-------|
| <0.04 | | undefined type | 0.028 | |
| | <0.4 | undefined type | 0.028 | |
| | | 0.4-0.8 | haptophytes | 0.028 |
| | | 0.8-1.0 | <i>Synechococcus</i> -like cyanobacteria | 0.032 |
| 0.04-3 | 0.4-2.4 | 1.0-1.3 | <i>Prochlorococcus</i> | 0.029 |
| | | 1.3-2.4 | diatoms | 0.042 |
| | >2.4 | undefined type | 0.028 | |
| >3 | | 50 % others Type+ 50 % diatoms | 0.035 | |

Figure 1 illustrates the monthly global distribution of marine phytoplankton types. Note that the large range of undefined type in the polar regions is caused by the limitations of satellite-derived data. In these polar regions, there are frequent missing values in satellite observations due to the low radiation levels during the winter months, which may lead to uncertainty regarding the phytoplankton types and BIO emissions in high-latitude regions. Development of inversion technique of remote data and marine observation are required to improve the BIO emission dataset in the high latitudes in the future. However, the impact of missing data in polar and subpolar regions is relatively limited, because previous studies indicated that isoprene is mostly emitted in the tropical and subtropical oceans in a trade-off relationship with dimethyl sulfide (DMS) (Dani and Loreto, 2017), which is also shown in our dataset. Therefore, despite the challenges posed by missing data in polar and subpolar regions, the overall estimation of global isoprene emissions is minimally affected when using undefined phytoplankton types in these areas.



200 **Figure 1: The spatial distribution of dominant phytoplankton types in January (a), April (b), July (c) and October (d) of 2012-2020. Six phytoplankton types are used here: 1 for undefined type, 2 for haptophytes, 3 for *Synechococcus*-like cyanobacteria, 4 for *Prochlorococcus*, 5 for diatoms and 6 for coastal type, which uses 50 % others type + 50 % diatoms.**

2.4 The SML emission module

205 The radiation intensity within a specific radiation band (280-400 nm) has been found as the factor determining the photochemistry-driven production and emission of isoprene according to the linear relationship between isoprene production and radiation intensity (Brüggemann et al., 2018). Here, following the parameterization of Brüggemann et al. (2018) and Conte et al. (2020), the equation below is used to estimate the marine photochemical emission of isoprene:

$$210 \quad F_s = F_{lab} \times \mu_{photo} \times S . \quad (6)$$

Where F_s ($\text{g} \cdot \text{grid}^{-1} \cdot \text{h}^{-1}$) is the flux of isoprene emissions from the SML. F_{lab} ($\text{molecules} \cdot \text{mW}^{-1} \cdot \text{s}^{-1}$) is the flux of isoprene from marine SML and biofilm measured in previous laboratory studies (Ciuraru et al., 2015b, a;



Brüggemann et al., 2017). $F_{lab} = 4.95 \times 10^7$ is used in this work, which represents the mean value within the range
(3.71×10^7 - 6.19×10^7) reported by Conte and Ciuraru (Ciuraru et al., 2015a; Conte et al., 2020). S (m^2) is the grid
215 cell area and μ_{photo} ($mW \cdot m^{-2}$) is radiation intensity between 280 and 400 nm reaching the surface of the ocean.
The calculation of μ_{photo} is determined by Eq. (7):

$$\mu_{photo} = E_{280-400} \times F_{surf} \times k_{SML} . \quad (7)$$

Where $E_{280-400}$ ($mW \cdot m^{-2}$) is determined to be 3.535 % of the surface downward solar radiation (Conte et al., 2020).
 F_{surf} represent the different surfactant concentrations in the SML defined as a ratio given by:

$$220 \quad F_{surf} = \frac{\ln(c_{surf})}{\ln(c_{max})} . \quad (8)$$

The two surfactant concentration terms, c_{surf} and c_{max} , are determined with a simplified method based on
previous research, using the concentration equivalents of Triton X as the surfactant concentration in SML (Wurl et
al., 2011). Here the nutrient level of the ocean is determined by the concentration of chlorophyll C_{chl} ($mg \cdot m^{-3}$). The
surfactant concentration reaches its maximum at $c_{max} = 663 \mu g \cdot Teq \cdot L^{-1}$ in eutrophic ocean with $C_{chl} \geq 0.4 mg \cdot m^{-3}$.
225 ³. A linear relationship was established to determine the surfactant concentration in the oligotrophic ocean with
 $C_{chl} < 0.4 mg \cdot m^{-3}$, which is $c_{surf} = 857 \cdot C_{chl} + 320 \mu g \cdot Teq \cdot L^{-1}$. The marine chlorophyll concentration data used in
the estimation of SML emissions is same as that used in the above estimation of BIO emissions.

The exchange velocity factor k_{SML} in Eq. (7) is calculated as the following equation (Mcgillis et al., 2004):

$$k_{SML} = \frac{8.2 + [0.014 \times w^3]}{8.2 + [0.014 \times w_{lab}^3]} , \quad (9)$$

230 where the parameter k_{SML} used in this study is normalized based on the work of Brüggemann et al. (2018) and
Ciuraru et al. (2015a, 2015b) with $w_{lab} = 5.31 \times 10^{-2} m \cdot s^{-1}$, which is derived from laboratory studies (Brüggemann
et al., 2018; Ciuraru et al., 2015b, a). w represents 10-metre windspeed. In addition, the SML emission is assumed
to occur only when the 10-metre windspeed is smaller than $13 m \cdot s^{-1}$ according to field observations (Brüggemann
et al., 2017; Brüggemann et al., 2018; Sabbaghzadeh et al., 2017).

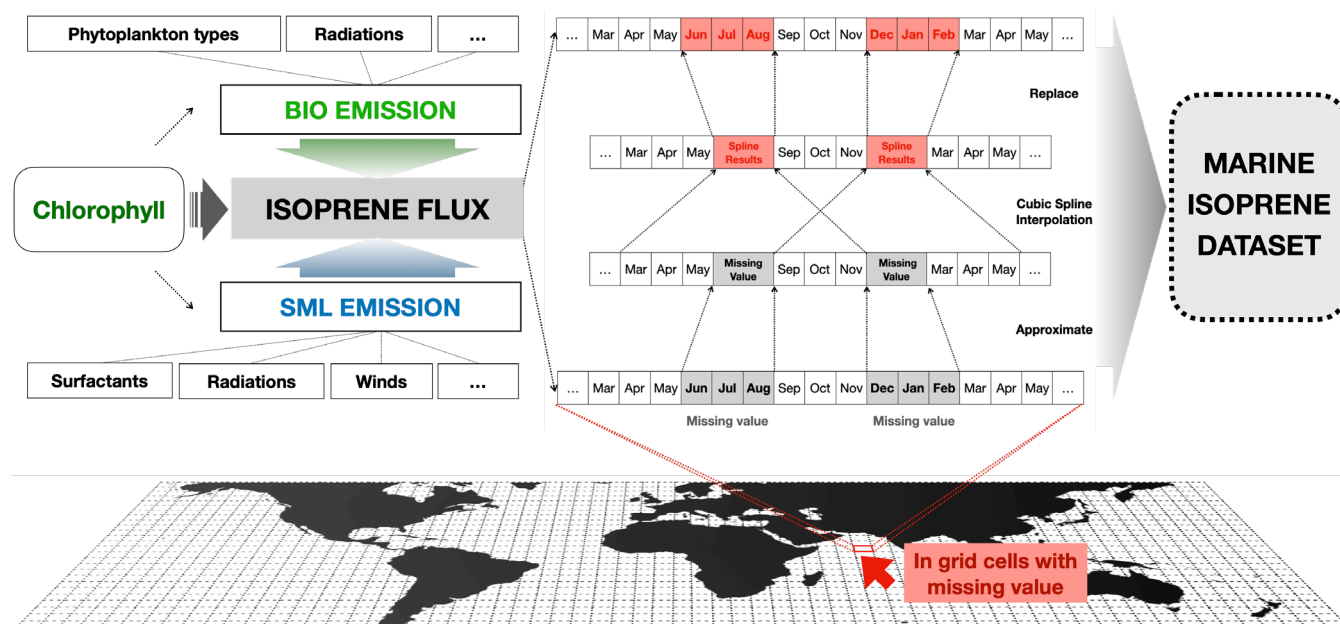
235 **2.5 Interpolation for missing values**

Due to the influence of dust aerosols and clouds, there are regions with missing data for marine chlorophyll
concentration, such as the North Arabian Sea and Gulf of Guinea ($30^\circ N$ - $30^\circ S$, 0° - $120^\circ E$) and the North Pacific
Subpolar Gyre ($60^\circ N$ - $30^\circ N$, $150^\circ E$ - $150^\circ W$) (Alvain et al., 2005; Alvain et al., 2008). Consequently, the



calculation of isoprene emissions using the aforementioned methods is not possible in these regions, leading to the
240 underestimation of global isoprene emissions. The missing value regions primarily exist in the tropic and subtropic
areas, where the seasonal variation of isoprene emission is limited. An interpolation for hourly isoprene BIO and
SML emission is applied during the boreal summer (June, July and August) and winter months (December,
November and January) in this study. This interpolation for the missing value area based on the emission in the
adjacent spring and fall months in the same grid. In the North Pacific region, missing values only occur in the
245 summer month, with an extent comparable to interpolated regions in the tropic and subtropic areas. The same
interpolation method is applied to fill the missing data and provide a basic emission status.

Figure 2 illustrates the interpolation process, which is an integral part of dataset establishment. This process entails
utilizing the hourly isoprene emission data to calculate the monthly average diurnal variation for each grid that
contains missing values. The cubic spline interpolation is then applied to determine the missing values in the
250 summer and winter months using adjacent spring and fall emission data. The interpolated area accounts for
approximately 3.1 % of the global ocean during the summer while 0.9 % during the winter. Overall, the
interpolation increases global isoprene emissions by 7.0 % in the summer, 3.4 % in the winter and 2.4 % for the
entire year.



255 **Figure 2: Calculation process of the estimation and interpolation method used in our dataset. Based on chlorophyll concentration and other meteorological factors, two types of isoprene emissions were included to determine the total marine isoprene emission flux. Cubic spline interpolation was used for grid cells with missing emission values during the period of boreal summer and winter.**



3 Evaluation and comparison

260 3.1 Comparison with observations

The accuracy of our method for estimating isoprene emission flux was assessed by comparing our isoprene emission dataset with previous cruise and inshore observations. Most of these results provide information on the range of isoprene concentration in the surface seawater of various regions, including Atlantic, Northern Pacific, East China Sea, Tropical Indian Ocean and Southern Ocean, while several results were derived from a single
265 sampling site with only a single value such as Tropical Pacific, Malaysia Peninsular and Mediterranean (Table 3). Furthermore, our work collected observed marine isoprene emission flux results from previous studies including four cruise researches and two inshore sites (Table 4). Most of these flux results were derived from calculations that involved the isoprene concentration in the seawater and the mixing ratio of isoprene in the marine boundary layer (method described below). Additionally, there was a floating flux chamber study conducted in the Peninsular
270 Malaysia coastal region to measure the isoprene flux directly (Uning et al., 2021) (Table 4).

The comparison of estimated isoprene emission flux and isoprene concentration in the seawater with the corresponding observations was performed in the respective regions and months. The comparison of emission fluxes was summarized in Fig. 3. The absolute value deviations between our estimated results and the observations range from 46.0 %~51.5 % in coastal regions and from 20.8 %~57.7 % in remote oceans. Among the six
275 comparisons, the largest deviation (57.7 %) was found in the North Atlantic region observed by Hackenberg et al. (2017) in boreal fall. However, our simulated emission flux showed a close agreement with another observation in the North Atlantic by Kim et al. (2017) with absolute value deviations of 20.8 %. It is important to note that various factors, such as occasional bloom events and the inherent variability of observations, may contribute to the differences observed in the same area.

280



Table 3: Observed marine isoprene concentrations in previous studies.

| Time | Location | Range ($\text{pmol} \cdot \text{L}^{-1}$) | References |
|-------------------|----------------------------|------------------------------------------------|---------------------------|
| 1990 Apr | South Pacific | 6.69-99.1 | (Bonsang et al., 1992) |
| 2010-2011 Dec-Jan | Southern Ocean | 0.2-348 | (Kameyama et al., 2014) |
| | Polar Northwest Pacific | 1.3-31 | |
| | Subpolar Northwest Pacific | 2.2-60 | |
| 2012 Sep-Oct | Transition Water | 6.4-165 | (Ooki et al., 2015) |
| | Subtropical Indian Ocean | 5.4-50 | |
| | Tropical Indian Ocean | 29-75 | |
| 2008 Nov | East Atlantic | 2-157 | (Booge et al., 2016) |
| 2013 Jul | East China Sea | 32.46-173.52 | (Li et al., 2017) |
| | South Yellow Sea | | |
| 2013 Oct-Nov | North Atlantic | 21 | (Kim et al., 2017) |
| 2012 Oct-Nov | North Atlantic | 8.75-63.26 | (Hackenberg et al., 2017) |
| 2013 Oct-Nov | North Atlantic | 1.12-38.20 | |
| 2013 Mar | Arctic | 1.96-10.57 | |
| 2013 Jul-Aug | Arctic | 3.86-66.38 | (Booge et al., 2018) |
| 2014 Jul-Aug | Indian Ocean | 6.1-27.1 | |
| 2014 Aug-Oct | West Pacific | 15.9-33.1 | |
| 2018 Jul | Zenibako coastal | 27.08-28 | (Li et al., 2020) |
| | Bering Sea | 21.36-67.73 | |
| 2017 Jul-Sep | Malaysia Peninsular | 8.3-34.3 | (Uning et al., 2021) |
| 2018 Apr-May | Southwest UK coast | 80-100 | (Phillips et al., 2021) |
| 2017 Jul | Davis Strait | 59 | (Wohl et al., 2022) |
| 2019 Jul-Aug | Southern Ocean | < 54.00 | (Zhou et al., 2022) |
| 2018 Apr | Tropical Pacific | 17.5 | (Simo et al., 2022) |
| 2014 Apr-May | Mediterranean | 25.1-39.0 | |
| 2014 Oct-Nov | Atlantic | 4.5-104.1 | |
| 2015 Jan-Feb | Southern Ocean | 6.3-64.2 | |



Table 4: Observed marine isoprene emission flux in previous studies.

| Time | Location | Range molecules · cm ⁻² · s ⁻¹ | Range (Monthly) mg · m ⁻² | Methods | References |
|----------------------|--------------------------|---------------------------------------------------------|-----------------------------------------|---------------------------------------------------------|----------------------------------------------|
| 2013 Oct-Nov | North Atlantic | 5.0E+7 | 0.15 | Eddy covariance method | (Kim et al., 2017) |
| 2017 Jul-Sep | Malaysia Peninsular | 19.4E+7 | 0.58 | Floating flux chamber TD-GC-MS | (Uning et al., 2021) |
| 2017 Apr-May | Arabian Sea | 1.5-12E+7 | 0.045-0.36 | Seawater isoprene concentration Exchange velocity | (Tripathi et al., 2020) |
| 2012&2013 Oct-Nov | Atlantic Ocean | 0.005-34E+7 | 0.0002-1.01 | | (Hackenberg et al., 2017) |
| Time | Location | Range nmol · m ⁻² · d ⁻¹ | Range (Monthly) mg · m ⁻² | Methods | References |
| 2001 May | Western North Pacific | 161.5 (22.17-537.2) | 0.34 (0.047-1.13) | Average isoprene mixing ratio | (Matsunaga et al., 2002; Li et al., 2017) |
| 2010-2011 Dec-Jan | South Ocean | 181-313 | 0.38-0.66 | Seawater isoprene concentration Exchange velocity | (Kameyama et al., 2014) |

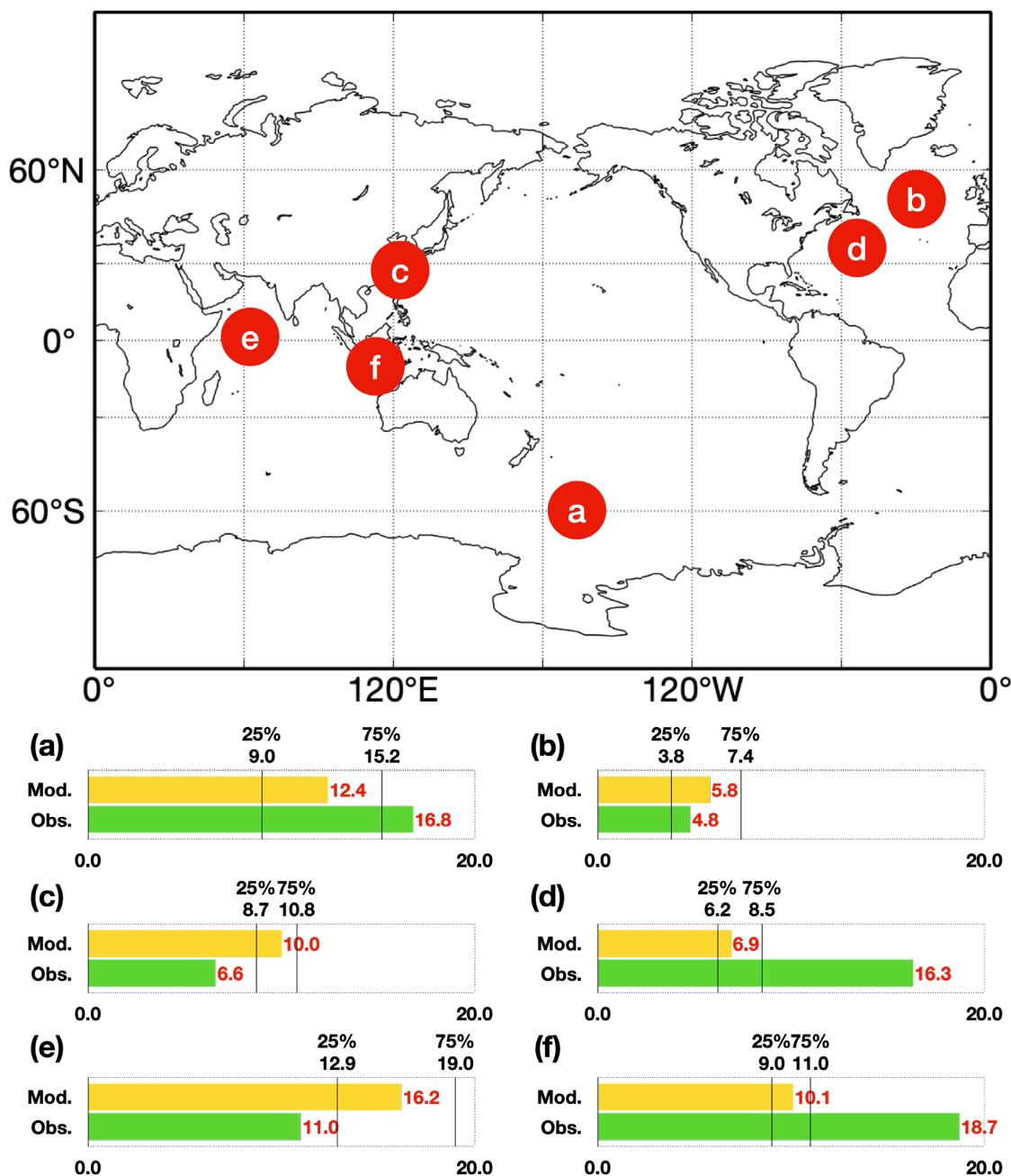


Figure 3: Comparisons between simulated isoprene emission fluxes (unit in $\mu\text{g}\cdot\text{m}^{-2}$) and observations. Yellow bar is daily mean isoprene emission flux in corresponding ocean regions. Two solid lines represent quartiles of the range for simulations. Green bar is the daily mean of observed emission flux. Six regions including the Southern Ocean (a) (Kameyama et al., 2014), North Atlantic (b and d) (Hackenberg et al., 2017; Kim et al., 2017), East China Sea and South Yellow Sea (c) (Li et al., 2017), Arabian Sea (e) (Tripathi et al., 2020) and Malaysia Peninsular (f) (Uning et al., 2021).

285

290



In our method, the isoprene emission flux is directly derived assuming equivalence with isoprene production, so the isoprene concentrations in seawater are not necessary to be explicitly calculated in the module described in Sect. 2. In order to compare with the observed isoprene concentration in the seawater, we calculated the seawater isoprene concentration by simulated isoprene emission flux and exchange velocity using the following equation:

$$C_{iso} = \frac{F_b + F_s}{k_{ex}} \quad (10)$$

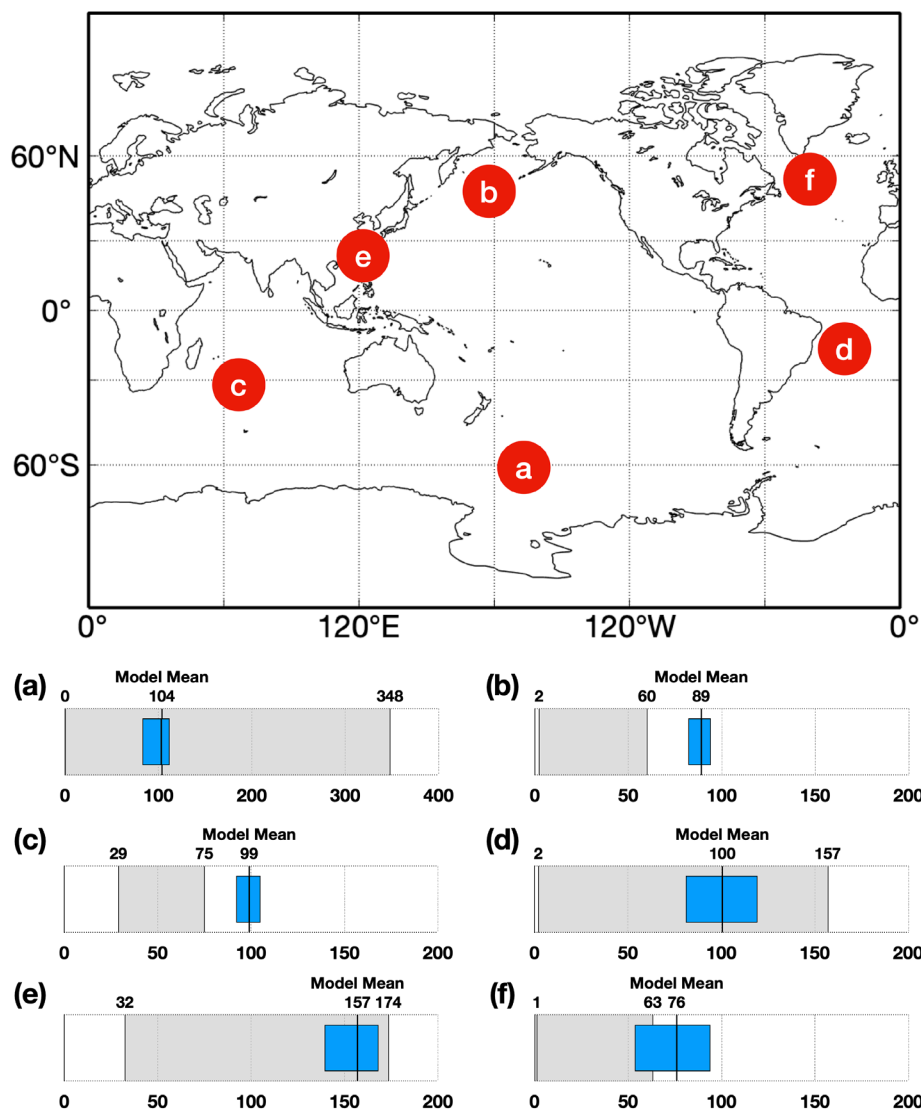
where F_b is BIO emissions flux. F_s is SML emissions flux. k_{ex} ($\text{cm}\cdot\text{h}^{-1}$) is the exchange velocity on the air-sea interface. The exchange velocity k_{ex} is determined by wind and sea surface temperature (Wanninkhof, 2014):

$$k_{ex} = \frac{0.31w^2}{\sqrt{\frac{Sc}{660}}} \quad (11)$$

where w is 10-metre windspeed. Notes that Eq. (11) is valid with w in the range of 4-15 $\text{m}\cdot\text{s}^{-1}$. Sc is Schmitt number determined by sea surface temperature (Wanninkhof, 2014):

$$Sc = 3913 - 162.13t + 2.67t^2 - 0.012t^3 \quad (12)$$

where t is the sea surface temperature in Celsius degree. The hourly 10-metre windspeed, sea surface temperature from reanalysis data and hourly isoprene emission flux from our dataset were used to calculate sea water isoprene concentration using Eq. (11). The comparisons between simulated isoprene concentrations and observations were conducted in six regions with different latitudes and various nutrient conditions (Fig. 4). The derived isoprene concentrations from our emission flux data have range overlapping the observations in Southern Ocean, Atlantic and Eastern China Sea, while the simulated isoprene concentrations in North Pacific and tropical Indian Ocean were overestimated by 32.0 % to 48.3 % compared to observations. The exchange velocity calculated using Eq. (11) may introduce uncertainty, which could partly explain the bias between simulation and observation. In addition, the constant factor of 0.31 in Eq. (11) and the Schmitt number Sc determined by Eq. (12) can vary depending on ocean conditions such as solute types and sea surface temperature, which may also contribute to the bias between simulations and observations.



315

320

Figure 4: Comparisons between simulated isoprene concentration (unit in $\text{pmol}\cdot\text{L}^{-1}$) and observations. Blue bar is the range (25-75 percentile) of simulated isoprene concentration in corresponding ocean region. The black solid line within the blue bar presents the mean of simulated isoprene concentration. Grey bar is the range of observed isoprene concentration. Six regions including the Southern Ocean (a) (Kameyama et al., 2014), Subpolar Pacific (b) (Ooki et al., 2015), Tropical Indian Ocean (c) (Ooki et al., 2015), East Atlantic (d) (Booge et al., 2016), East China Sea and South Yellow Sea (e) (Li et al., 2017) and North Atlantic (f) (Hackenberg et al., 2017).



3.2 Comparison with previous estimation results

325 The average annual isoprene emissions for the period of 2001-2020 are estimated to be $1.049 \text{ Tg}\cdot\text{yr}^{-1}$, with range
of $1.030\text{-}1.063 \text{ Tg}\cdot\text{yr}^{-1}$ using our module. Thereinto, the annual global BIO emissions range is $0.419\text{-}0.443 \text{ Tg}\cdot\text{yr}^{-1}$,
¹, which corresponds to the total emissions from various types of phytoplankton. The annual global SML emissions
result is in the range of $0.611\text{-}0.621 \text{ Tg}\cdot\text{yr}^{-1}$, which is generated by photochemical processes in the SML.

In previous studies, several model-based estimations of marine isoprene emissions were conducted, as summarized
330 in Table 1. Most of these studies utilized a bottom-up approach, while a few employed a top-down approach. There
is a significant difference in the estimated isoprene emissions between these two methods. Top-down estimations
generally yielding larger values compared to bottom-up estimations. This difference can be attributed, in part, to
the exclusion of high-emission events and hotspots in bottom-up methods (Yu and Li, 2021). The missing values
of the source data and the unclear mechanisms of marine isoprene production, consumption and sea-air exchange
335 all lead to the uncertainty using bottom-up method (Conte et al., 2020; Gantt et al., 2009; Hackenberg et al., 2017;
Palmer and Shaw, 2005; Yu and Li, 2021). On the other hand, the limited observation datasets and insufficient
spatial resolutions of input data decrease the accuracy of current top-down results (Arnold et al., 2009; Luo and
Yu, 2010). Additionally, the air-sea exchange flux of marine isoprene, which is used in top-down methods, cannot
be directly observed, further contributing to the uncertainty in these approaches. Furthermore, most of the available
340 isoprene flux observations are conducted at inshore sites, which may not be suitable for estimating emissions in
remote ocean areas (Simo et al., 2022). Based on the previous estimate method, our work has applied several
improvements to our bottom-up method to address the existing gaps and discrepancies between top-down and
bottom-up results. These improvements are discussed in detail in the next section.

3.3 Model improvements and comparisons

345 In our model, we implemented several ways to improve the estimation of global BIO and SML emissions compared
to previous datasets. These improvements include updates to the methods and an increase in temporal and spatial
resolution. The temporal resolution of the dataset was enhanced to one hour, allowing for a more detailed
examination of the diurnal and seasonal variations of isoprene emissions to capture short-term changes and events
that may influence emissions, which probably provides a more accurate representation of emission dynamics. The
350 spatial resolution was set to $0.25^\circ\times 0.25^\circ$, which is consistent with the spatial resolution of ERA5 reanalysis data.
This fine spatial resolution allows for a more precise representation of the spatial distribution of isoprene emissions,
particularly in coastal regions where emission patterns vary significantly. The phytoplankton types distribution



scheme used in BIO emission calculation has been updated and simplified based on the normalized water-leaving radiation at 410 nm and chlorophyll concentration data, according to previous work by (Alvain et al., 2005; Alvain et al., 2008). This update helps to avoid the issue of missing phytoplankton types within a number of grid cells in coastal regions, leading to a substantial improvement in the accuracy of emission estimation in these specific areas. Moreover, a latest parameterization (in Eq. (2)) was developed to estimate the biochemical consumption based on observations by Simo et al. (2022) with an upper limit of 0.373 when the chlorophyll concentration was larger than $5.77 \text{ mg}\cdot\text{m}^{-3}$. These improvements help to reduce the uncertainty of BIO emission estimation and enable to examine the characteristics of BIO emission in high spatial and temporal resolution.

The estimation of SML emissions was based on the radiation, windspeed and surfactants in the sea surface microlayer. Here we used chlorophyll concentration to determine the quantity of surfactants based on field measurement by Wurl et al. (2011), instead of the net primary production used in Brüggemann et al. (2018). This simplification of the model eliminates potential inconsistencies that may arise from using different datasets (chlorophyll concentration and net primary production) to describe the nutrient levels of the ocean. Mean surfactant concentrations are determined to be $c_{max} = 663 \text{ }\mu\text{g}\cdot\text{Teq}\cdot\text{L}^{-1}$ for eutrophic regions where the chlorophyll concentration is higher than $0.4 \text{ mg}\cdot\text{m}^{-3}$, while $c_{surf} = 857\cdot C_{chl} + 320 \text{ }\mu\text{g}\cdot\text{Teq}\cdot\text{L}^{-1}$ for oligotrophic regions.

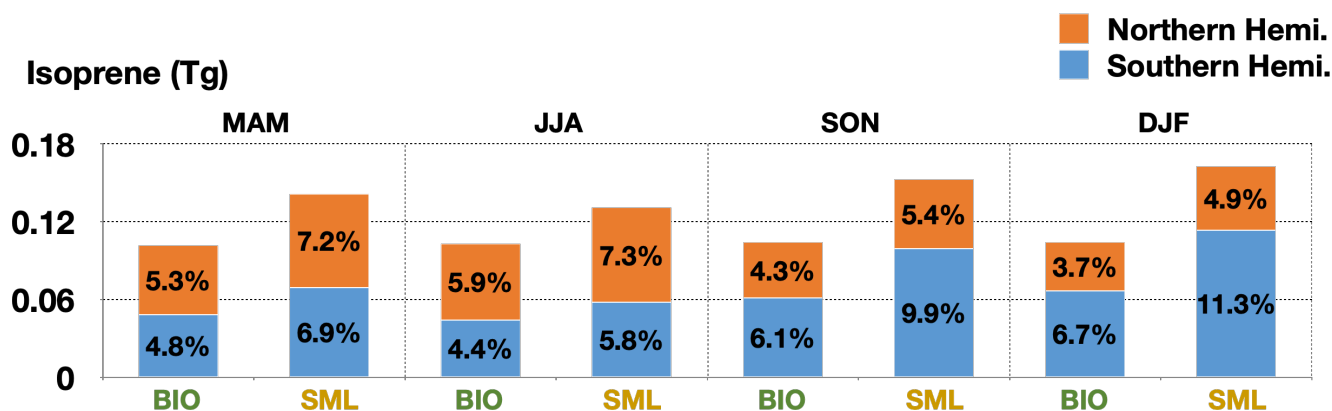
4 Results

4.1 Spatial and temporal distribution of marine isoprene emissions

Generally, our dataset suggests annual global marine isoprene emissions ranging from 1.030 to $1.063 \text{ Tg}\cdot\text{yr}^{-1}$ for the period 2001-2020, with an average of $1.049 \text{ Tg}\cdot\text{yr}^{-1}$ over the twenty years. Two typical marine isoprene emission processes were considered in our dataset, which are BIO emissions from phytoplankton biogenic generation and SML emissions through photochemical processes in the sea surface microlayer. Annual average global BIO emissions for the twenty-year period were $0.433 \text{ Tg}\cdot\text{yr}^{-1}$, ranging from 0.419 to $0.443 \text{ Tg}\cdot\text{yr}^{-1}$, while annual average global SML emissions was $0.616 \text{ Tg}\cdot\text{yr}^{-1}$, ranging from 0.611 to $0.621 \text{ Tg}\cdot\text{yr}^{-1}$. In the twenty-year period, the average annual emissions in the Northern Hemisphere amounted to approximately 44.1 %, whereas the Southern Hemisphere accounted for 55.9 % of the total emissions. A significant difference in total emissions between the hemispheres, particularly during boreal winter (Fig. 5). Based on our twenty-year data, the emission in the boreal winter of the Southern Hemisphere contributed 18.0 % of annual global emissions in average, while the emission in the same season of the Northern Hemisphere accounted for only 8.6 %. This highlights the unneglectable importance and dominance of marine isoprene emissions in the Southern Hemisphere compared to



the Northern Hemisphere, suggesting potential environmental impacts and climate modifications associated with these emissions.



385 **Figure 5: Seasonal variation of the contribution of BIO and SML emissions from two hemispheres to annual global emissions for the period 2001-2020.**

Based on the datasets, we can find distinct spatial characteristics in marine isoprene emissions at a global scale, revealing specific patterns in annual emissions (Fig. 6). The BIO emissions are closely linked to chlorophyll concentration, exhibiting a similar spatial pattern to marine chlorophyll (Fig. 6a, 6c). Regions such as coastal areas, convergence zones, and upwelling areas (e.g., East China Sea, tropical Pacific, Offshore Peru) exhibit high BIO emissions due to the presence of elevated chlorophyll concentrations and abundant nutrients. These conditions may arise from anthropogenic eutrophication in coastal areas or the natural flow of ocean current systems (Dai et al., 2023). The emission rates in coastal areas is significantly larger than the remote ocean by several orders of magnitude. However, the emission from the remote ocean still dominates global marine isoprene emissions due to the vast surface area of remote ocean regions. Additionally, there is evidence of an increased frequency of potential phytoplankton bloom events, particularly in coastal regions and the Southern Ocean, over the past two decades (Dai et al., 2023). SML emissions are determined mathematically using radiation, windspeed and surfactant concentration. Consequently, our results indicate that the high emission frequently presents in the subtropical ocean with ample radiation and large windspeed, as well as eutrophic coastal regions (Fig. 6a, 6b).

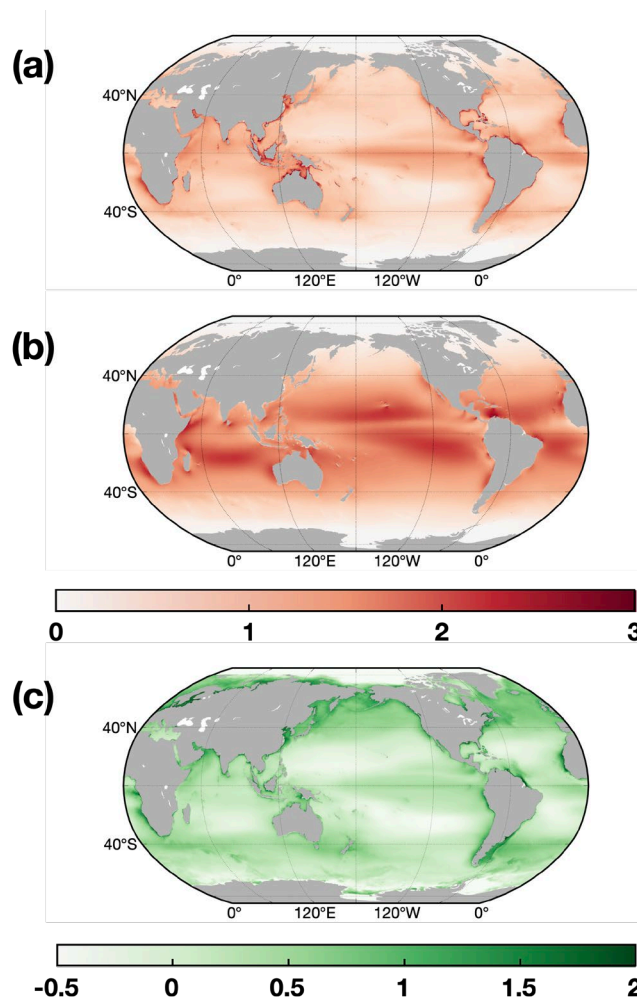
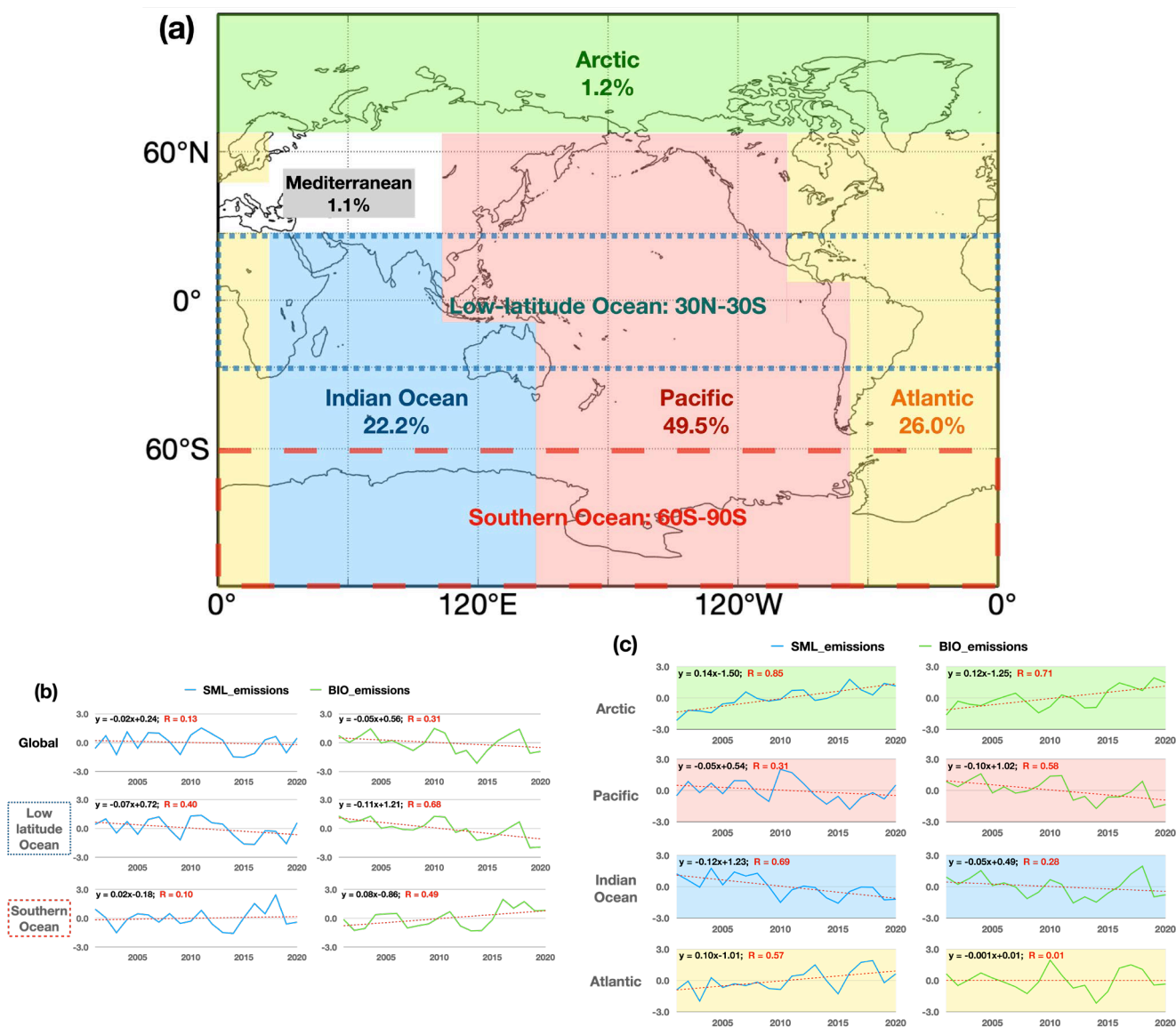


Figure 6: Mean annual BIO emissions (a), annual SML emissions (b) (unit in t), and annual Chlorophyll-a concentration (c) (in log₁₀ coordinates) for twenty years.

405 The annual average global marine isoprene BIO and SML emissions exhibit a slight decreasing trend over the last
twenty years (Fig. 7b). However, the emission trends vary significantly among different ocean regions. The annual
emission from Pacific (49.5 %) and Indian Ocean (22.2 %) contributes 71.7 % to the global isoprene emission and
emissions in both regions were decreasing in the last twenty years (Fig. 7a). In contrast, the Arctic Ocean shows
an increasing trend in annual emissions, although its contribution to the global marine isoprene emission is only
410 1.2 % (Fig. 7a, 7c). The emissions in the low latitude ocean are most important over the global marine isoprene
emission attributed by the intense radiation, and high concentration of chlorophyll relative to subtropical remote
ocean, which account for 36.7 % of global marine isoprene emission. The SML emission in low latitudes was



decreased by 5.6 % per year while the BIO emission was decreased by 3.0 % per year over the twenty-year period (Fig. 7a, 7b).



415

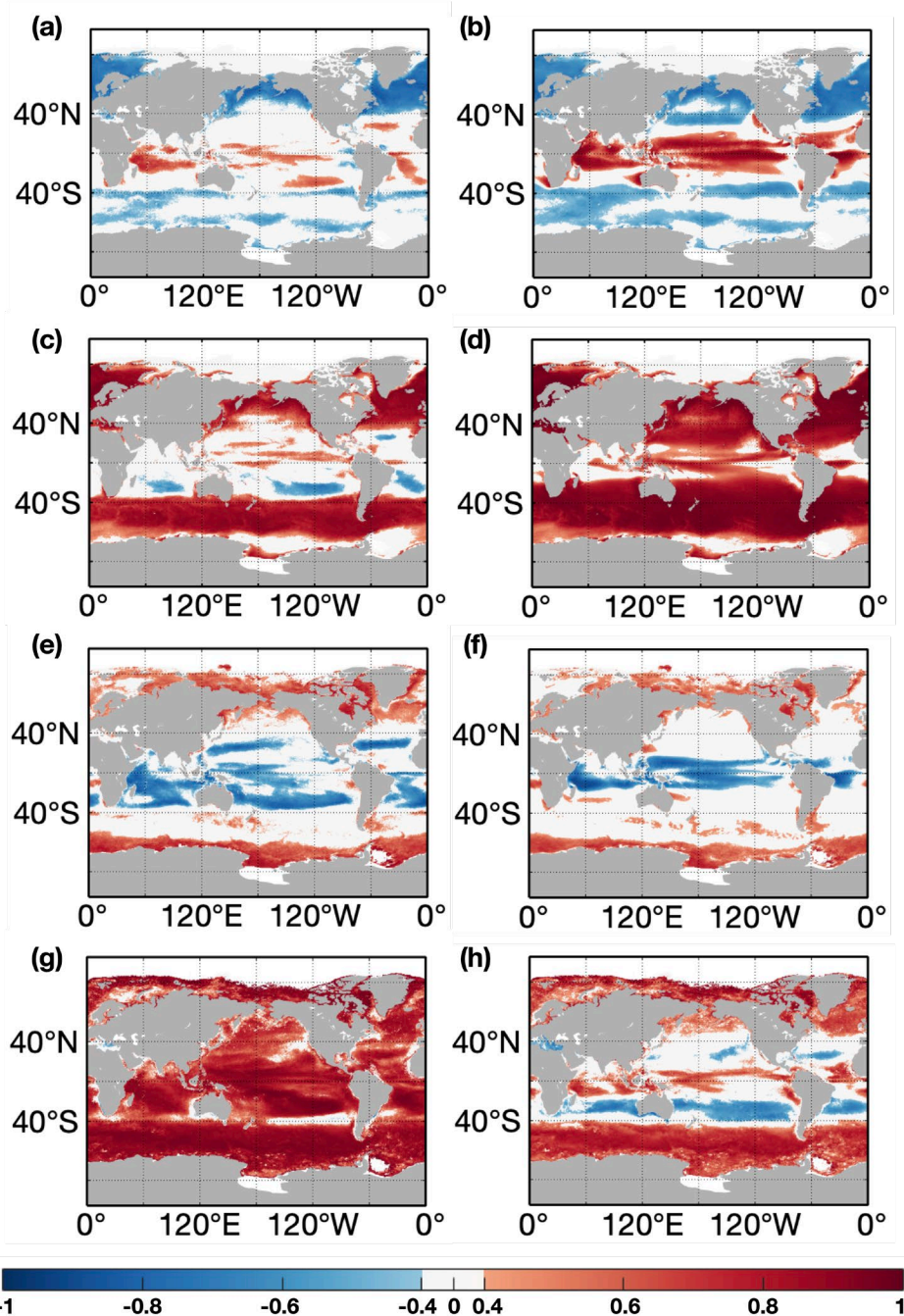
420

Figure 7: Twenty-year mean contributions of annual isoprene emissions from different ocean regions to global annual emissions (a) and standardized trends of two types of annual isoprene emissions in different ocean regions (b, c).



4.2 Influence of marine and meteorological factors

The variations of isoprene emissions are primarily influenced by marine and meteorological conditions, both directly and indirectly. The effects of four dominant factors including 10-metre windspeed, surface downward solar radiation, sea surface temperature and marine chlorophyll concentration, were examined by correlating them with BIO and SML emissions (Fig. 8). Chlorophyll concentration is considered a factor that quantifies nutrient levels and phytoplankton activities, which also was used to determine the surfactant content in the sea surface microlayer. Globally, chlorophyll concentration has a significant positive correlation ($r = 0.67$, $p \leq 0.05$) with BIO emissions (Fig. 8g). However, chlorophyll concentration shows positive correlation with SML emissions in the polar, subpolar and tropical regions, while negative correlation in the subtropical region, suggesting that other critical factors control SML emissions in these areas (Fig. 8h). Surface solar radiation downward is another important factor influencing both BIO emissions and SML emissions. There is a globally positive correlation between surface solar radiation downward and SML emissions (Fig. 8d), with a significant coefficient of $r = 0.62$ ($p \leq 0.05$) in the global average, while positive correlations with BIO emissions are only found on mid and high latitudes beyond 40°N and 40°S (Fig. 8c). Sea surface temperature and 10-metre windspeed have less impact on BIO and SML emissions compare to the other two factors in most open ocean areas. Large number of grid cells with weak correlations ($|r| \leq 0.4$) and correlations that did not pass our significance test ($p > 0.05$) for sea surface temperature and 10-metre windspeed with BIO and SML emissions are shown in Fig. 8 (Fig. 8a, 8b, 8e, 8f). These two physical factors affect marine isoprene emissions indirectly by altering the air-sea exchange processes, and show contrasting correlations, especially in tropical ocean (Fig. 8a, 8b, 8e, 8f), where BVOCs emission is determined by local air-sea system (Xu et al., 2016). The variations of marine and meteorological factors are all the result of variation of air-sea system, suggesting that the variability of large-scale air-sea system may contribute to the variability in marine isoprene emissions (Abbatt et al., 2019; Hackenberg et al., 2017; Xu et al., 2016; Zhang and Gu, 2022).



445 **Figure 8: Correlation coefficients of 10-metre windspeed (a, b), surface solar radiation downward (c, d), sea surface temperature (e, f) and chlorophyll concentration (g, h) with BIO emissions (a, c, e, g) and with SML emissions (b, d, f, h). Note that the grids where the absolute values of correlation coefficients are above 0.4 ($P \leq 0.05$) are filled with colours.**



4.3 Potential effects of the air-sea system

In order to investigate the potential impact of air-sea systems on isoprene emissions and identify the specific target area, the multiple variables empirical orthogonal function (MVEOF) was employed to examine the spatial pattern of temporal variation in BIO and SML isoprene emissions (Fig. 9). From a global perspective, the leading MVEOF principal component (41.26 % explained variance) reveals a seasonal periodicity in both types of emissions, with a symmetrical pattern between the two hemispheres (Fig. 9a-d). In addition, the other principal components do not exhibit any distinct or meaningful spatial patterns. The same analysis method was used to identify the leading potential pattern for the tropical and subtropical regions (30° N-30° S) (Fig. 9e-f). In this case, two leading EOF modes are presented, with the sum of explained variances of 37.28 %. The first mode suggests that BIO and SML emissions have different spatial pattern, in which the BIO emissions show potential opposite patterns between the coastal and remote ocean regions. The second leading mode reveals a distinct signal in the Indian Ocean, characterized by a symmetric pattern resembling the Indian Ocean Dipole (IOD), which is a dominant quasi-periodic variation in sea surface temperature in the Indian Ocean. For SML emissions, the first mode shows an El Niño-Southern Oscillation (ENSO)-like spatial pattern in the tropical Pacific. This suggests a connection between annual and seasonal variations in isoprene emissions and the large-scale air-sea system variability. It is likely that marine isoprene emissions are influenced by air-sea interactions, including ENSO and other climate patterns at various scales. Previous studies have also found increased marine DMS emissions in the tropical Pacific during La Niña events due to anomalies in sea surface winds (Xu et al., 2016).

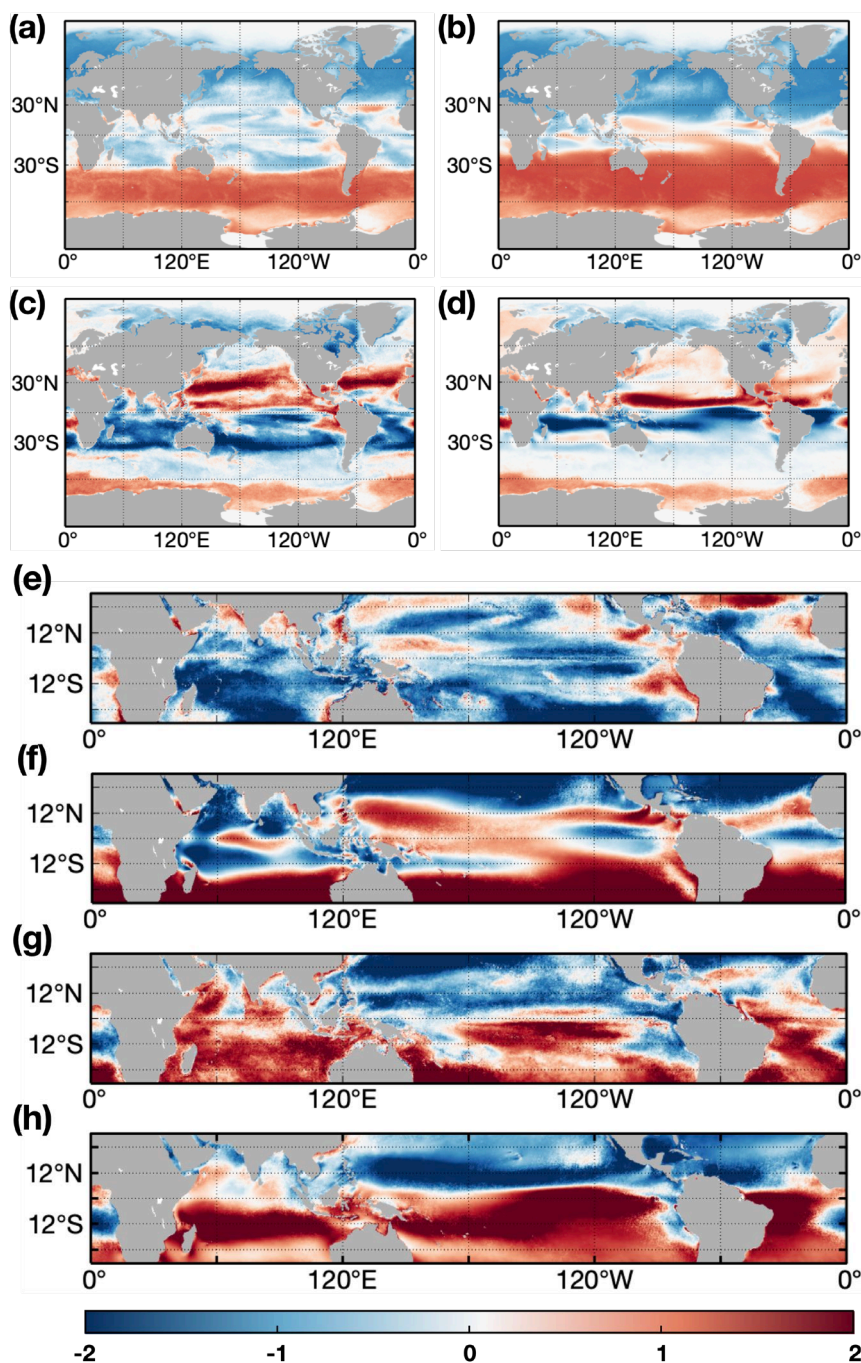
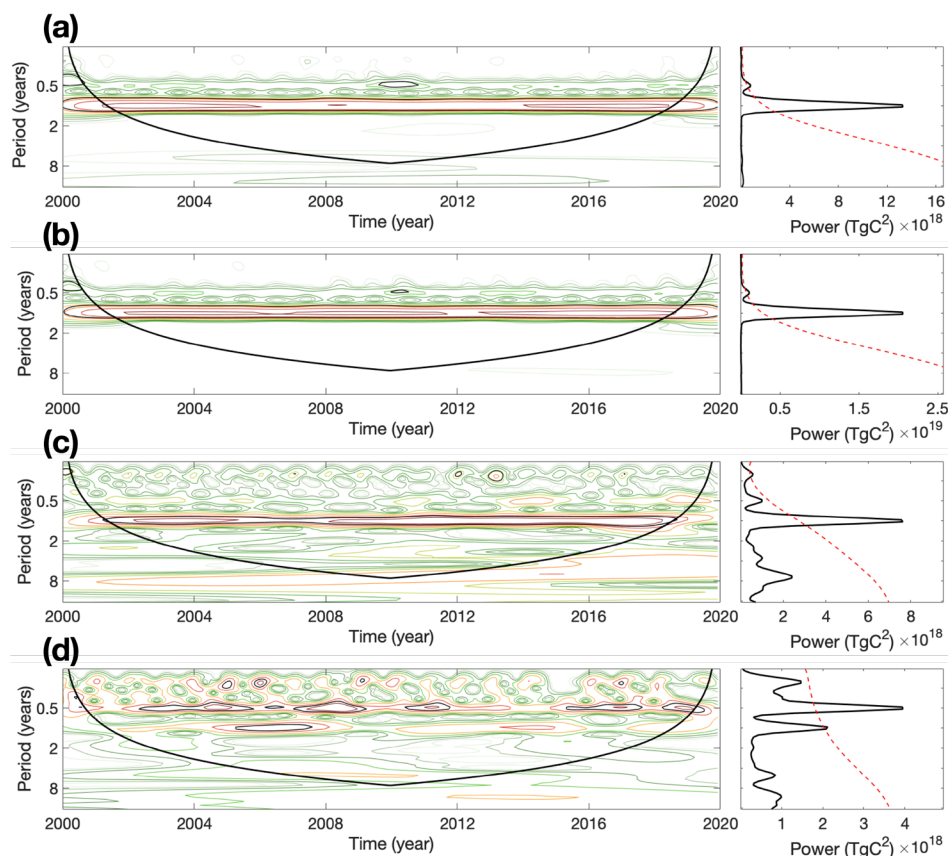


Figure 9: MVEOF results for global emission (a-d) and low latitude (30° N-30° S) emission (e-h). a-b and e-f is the first two mode of BIO emission, c-d and g-h is the first two mode of SML emission. In the global extent, the explained variances for leading two modes are 41.26 % and 9.99 %. In the low latitudes, the explained variances for leading two modes are 20.75 % and 16.53 %. The amplitudes are in tons.

470



To further investigate the periodic changes in isoprene emissions and identify corresponding air-sea systems with similar cycles, wavelet analysis was applied to the monthly data. This analysis allowed us to identify significant periods in different regions. At the global scale, interannual variability is the most common and prominent for both
475 BIO emissions and SML emissions (Fig. 10). This annual signal is largely influenced by the solar radiation cycle. Besides, a half-year period was derived from the mid-latitude and tropical SML emissions. The same period was also observed for BIO emissions. Furthermore, a significant intraseasonal period was found in the tropical Indian Ocean and the tropical Pacific (Fig. 10c). This period, shorter than a season (0.25 years), occurs almost every year and is believed to be associated with the Madden-Julian Oscillation (MJO). The MJO is a dominant component of
480 tropical intraseasonal variability and is associated with the large-scale signal of deep convection, which strongly affects precipitation and radiation in the tropical ocean area. The periodic information is a potential indicator to find and link emission variations and driver changes. These identified periods demonstrate the potential relationships between marine isoprene emissions and variations in the air-sea system.



485 **Figure 10: Wavelet power spectrum and time averaged wavelet spectrum of BIO emission (a and c) and SML emission (b and d) of mid latitude Pacific (a-b) and tropical Indian Ocean and Pacific (c-d).**



4.4 Data uncertainties

The uncertainties in our model primarily presence in the parameterizations of various physical and biochemical processes. Since the linear relationship between isoprene emission and phytoplankton biomass is not universally applicable in all situations (Kameyama et al., 2014), a large size of measurement is required at higher spatial and temporal resolution to improve the parameterizations. Add to that, the column concentration of chlorophyll was derived from satellite observation in our module with the assumption that chlorophyll is well mixed in the euphotic layer, although satellite is only able to detect the chlorophyll concentration on the surface of ocean. The isoprene productions in our model are determined by integrating over depth, taking into account the radiation levels that control the isoprene emission rate at different depths. However, previous studies indicated that the highest isoprene concentrations may occur below the surface, often coinciding with the maximum chlorophyll concentrations (Conte et al., 2020; Wohl et al., 2022). As a result, uncertainty in the vertical distributions of chlorophyll and isoprene concentration under sea surface microlayer may lead to the uncertainty in the estimation of marine isoprene emission. Furthermore, previous observations detected notable VOCs emissions in the Arctic region and high-latitude South Ocean during winter (Abbatt et al., 2019; Wohl et al., 2023). These emissions may be underestimated in our model due to the limitations of satellite data. Moreover, observations have indicated that isoprene production in the ocean occurs even when phytoplankton are covered by sea ice. As a result, high marine isoprene concentrations were measured in the ice edge waters and melted ponds (Wohl et al., 2022; Abbatt et al., 2019; Wohl et al., 2023). The accumulated isoprene under sea ice is emitted once the ice melts, which process was not included in our module.

5 Data availability

Hourly global marine isoprene BIO and SML emission dataset at a spatial resolution of $0.25^{\circ} \times 0.25^{\circ}$ from 2001 to 2020 can be accessed directly through: <http://dx.doi.org/10.11888/Atmos.tpsc.300521> (Cui and Zhu., 2023).

6 Conclusions and Perspective

In this work, a new marine isoprene emission module was built to generate a dataset of marine isoprene emissions with improved spatial and temporal resolution. This was achieved by incorporating comprehensive parameterized solutions based on remote sensing data on ocean chlorophyll concentration and reanalysis of climate data. The module considers separate parameterizations for BIO emissions and SML emissions, taking into account different



physical processes. Our module estimate the total global marine isoprene emissions to be $1.049 \text{ Tg}\cdot\text{yr}^{-1}$ on average
515 over a twenty-year period, with $0.433 \text{ Tg}\cdot\text{yr}^{-1}$ attributed to BIO emissions and $0.616 \text{ Tg}\cdot\text{yr}^{-1}$ to SML emissions. To
validate our results, several observations of marine isoprene concentrations and emission fluxes were collected for
comparison with our results. These comparisons demonstrate the reasonableness and consistency of our data.
Using the hourly data, we conducted a detailed analysis of the spatial and temporal distributions of marine isoprene
emissions, including their trends and periodic characteristics. On a global scale, significant disparities and
520 variations in emissions between the Southern Hemisphere and the Northern Hemisphere have been observed,
displaying distinct seasonal patterns. The emissions from the Southern Hemisphere play a crucial role, particularly
during the boreal winter, while the emissions in the Northern Hemisphere amount to only half of those in the
Southern Hemisphere. Isoprene emissions are unevenly distributed across various ocean regions. Eutrophic ocean
areas, such as coastal regions and eastern boundary current systems, consistently demonstrate higher marine
525 isoprene emissions compared to remote oligotrophic ocean areas, often by orders of magnitude. We identified a
slight decreasing trend in global annual isoprene emissions over the 2001-2020 period, which is dominated by a
significant decrease trend at low latitudes. Through wavelet analysis, multiple significant periods of isoprene
emissions are found, including annual, semi-annual and intraseasonal periods in different ocean regions. Several
periodic and quasi-periodic signals appear in the tropical and subtropical Indian Ocean and Pacific. These findings
530 indicate that air-sea systems drive isoprene emissions, particularly in the tropical and subtropical Indian Ocean and
Pacific regions. These quasi-periodic patterns and their relationships with emissions provide valuable insights for
refining existing methods and improving the accuracy of isoprene emission estimations. They also help bridge the
gap and reconcile discrepancies between observations and model calculations.

Author Contribution

535 JZ conceived the research; LC and JZ designed the module, performed emission module runs, created the emission
dataset and analyzed the data. YX contributed to the preparation of module input and data processing; YX, WH,
LS, YW, CZ and PF joined the discussion of the research and offered advice; LC wrote the first draft of the
manuscript; JZ and LC revised the manuscript before submission with contributions from all co-authors.

Competing interests

540 The authors have declared that they have no conflict of interest.



Acknowledgement

The monthly normalized water-leaving radiance data at 410 nm for the period of 2012-2020 were provided by NOAA's Center for Satellite Applications and Research (STAR) and the CoastWatch program.

Financial support

545 This research has been supported by supported by National Key R&D Plan(Grant No.2022YFF0803000) and National Natural Science Foundation of China (Grant No. 42177082).

References

- Abbatt, J. P. D., Leaitch, W. R., Aliabadi, A. A., Bertram, A. K., Blanchet, J. P., Boivin-Rioux, A., Bozem, H., Burkart, J., Chang, R. Y. W., Charette, J., Chaubey, J. P., Christensen, R. J., Cirisan, A., Collins, D. B., Croft, B., Dionne, J., Evans, G. J., Fletcher, C. G., Gali, M., Ghahreman, R., Girard, E., Gong, W. M., Gosselin, M., Gourdal, M., Hanna, S. J., Hayashida, H., Herber, A. B., Hesarakı, S., Hoor, P., Huang, L., Hussherr, R., Irish, V. E., Keita, S. A., Kodros, J. K., Kollner, F., Kolonjari, F., Kunkel, D., Ladino, L. A., Law, K., Levasseur, M., Libois, Q., Liggio, J., Lizotte, M., Macdonald, K. M., Mahmood, R., Martin, R. V., Mason, R. H., Miller, L. A., Moravek, A., Mortenson, E., Mungall, E. L., Murphy, J. G., Namazi, M., Norman, A. L., O'Neill, N. T., Pierce, J. R., Russell, L. M., Schneider, J., Schulz, H., Sharma, S., Si, M., Staebler, R. M., Steiner, N. S., Thomas, J. L., von Salzen, K., Wentzell, J. J. B., Willis, M. D., Wentworth, G. R., Xu, J. W., and Yakobi-Hancock, J. D.: Overview paper: New insights into aerosol and climate in the Arctic, *Atmos Chem Phys*, 19, 2527-2560, <https://doi.org/10.5194/acp-19-2527-2019>, 2019.
- Alvain, S., Moulin, C., Dandonneau, Y., and Breon, F. M.: Remote sensing of phytoplankton groups in case 1 waters from global SeaWiFS imagery, *Deep-Sea Res Pt I*, 52, 1989-2004, <https://doi.org/10.1016/j.dsr.2005.06.015>, 2005.
- 560 Alvain, S., Moulin, C., Dandonneau, Y., and Loisel, H.: Seasonal distribution and succession of dominant phytoplankton groups in the global ocean: A satellite view, *Global Biogeochem Cy*, 22, Artn Gb3001 <https://doi.org/10.1029/2007gb003154>, 2008.
- Arnold, S. R., Spracklen, D. V., Williams, J., Yassaa, N., Sciare, J., Bonsang, B., Gros, V., Peeken, I., Lewis, A. C., Alvain, S., and Moulin, C.: Evaluation of the global oceanic isoprene source and its impacts on marine organic carbon aerosol, *Atmos Chem Phys*, 9, 1253-1262, <https://doi.org/10.5194/acp-9-1253-2009>, 2009.
- 565 Booge, D., Schlundt, C., Bracher, A., Endres, S., Zancker, B., and Marandino, C. A.: Marine isoprene production and consumption in the mixed layer of the surface ocean - a field study over two oceanic regions, *Biogeosciences*, 15, 649-667, <https://doi.org/10.5194/bg-15-649-2018>, 2018.



- 570 Bonsang, B., Polle, C., & Lambert, G. (1992). Evidence for marine production of isoprene. *Geophysical Research Letters*, 19(11), 1129-1132. <https://doi.org/10.1029/92GL00083>, 1992
- Booge, D., Marandino, C. A., Schlundt, C., Palmer, P. I., Schlundt, M., Atlas, E. L., Bracher, A., Saltzman, E. S., and Wallace, D. W. R.: Can simple models predict large-scale surface ocean isoprene concentrations? *Atmos Chem Phys*, 16, 11807-11821, <https://doi.org/10.5194/acp-16-11807-2016>, 2016.
- 575 Brüggemann, M., Hayeck, N., and George, C.: Interfacial photochemistry at the ocean surface is a global source of organic vapors and aerosols, *Nat Commun*, 9, ARTN 2101 <https://doi.org/10.1038/s41467-018-04528-7>, 2018.
- Brüggemann, M., Hayeck, N., Bonninau, C., Pesce, S., Alpert, P. A., Perrier, S., Zuth, C., Hoffmann, T., Chen, J. M., and George, C.: Interfacial photochemistry of biogenic surfactants: a major source of abiotic volatile organic compounds, *Faraday Discuss*, 200, 59-74, <https://doi.org/10.1039/c7fd00022g>, 2017.
- 580 Carslaw, K. S., Boucher, O., Spracklen, D. V., Mann, G. W., Rae, J. G. L., Woodward, S., and Kulmala, M.: A review of natural aerosol interactions and feedbacks within the Earth system, *Atmos Chem Phys*, 10, 1701-1737, <https://doi.org/10.5194/acp-10-1701-2010>, 2010.
- Ciuraru, R., Fine, L., van Pinxteren, M., D'Anna, B., Herrmann, H., and George, C.: Unravelling New Processes at Interfaces: Photochemical Isoprene Production at the Sea Surface, *Environ Sci Technol*, 49, 13199-13205, <https://doi.org/10.1021/acs.est.5b02388>, 2015a.
- 585 Ciuraru, R., Fine, L., van Pinxteren, M., D'Anna, B., Herrmann, H., and George, C.: Photosensitized production of functionalized and unsaturated organic compounds at the air-sea interface, *Sci Rep-Uk*, 5, ARTN 12741 <https://doi.org/10.1038/srep12741>, 2015b.
- 590 Claeys, M., Wang, W., Ion, A. C., Kourtchev, I., Gelencser, A., and Maenhaut, W.: Formation of secondary organic aerosols from isoprene and its gas-phase oxidation products through reaction with hydrogen peroxide, *Atmos Environ*, 38, 4093-4098, <https://doi.org/10.1016/j.atmosenv.2004.06.001>, 2004.
- Conte, L., Szopa, S., Aumont, O., Gros, V., and Bopp, L.: Sources and Sinks of Isoprene in the Global Open Ocean: Simulated Patterns and Emissions to the Atmosphere, *J Geophys Res-Oceans*, 125, ARTN e2019JC015946 <https://doi.org/10.1029/2019JC015946>, 2020.
- 595 Dai, Y., Yang, S., Zhao, D., Hu, C., Xu, W., Anderson, D. M., Li, Y., Song, X.-P., Boyce, D. G., Gibson, L., Zheng, C., and Feng, L.: Coastal phytoplankton blooms expand and intensify in the 21st century, *Nature*, 615, 280-284, <https://doi.org/10.1038/s41586-023-05760-y>, 2023.
- Dani, K. G. S. and Loreto, F.: Trade-Off Between Dimethyl Sulfide and Isoprene Emissions from Marine Phytoplankton, *Trends Plant Sci*, 22, 361-372, <https://doi.org/10.1016/j.tplants.2017.01.006>, 2017.
- 600 Gantt, B., Meskhidze, N., and Kamykowski, D.: A new physically-based quantification of marine isoprene and primary organic aerosol emissions, *Atmos Chem Phys*, 9, 4915-4927, <https://doi.org/10.5194/acp-9-4915-2009>, 2009.



- Gantt, B., Xu, J., Meskhidze, N., Zhang, Y., Nenes, A., Ghan, S. J., Liu, X., Easter, R., and Zaveri, R.: Global distribution and climate forcing of marine organic aerosol - Part 2: Effects on cloud properties and radiative forcing, *Atmos Chem Phys*, 12, 6555-6563, <https://doi.org/10.5194/acp-12-6555-2012>, 2012.
- 605 Guenther, A., Karl, T., Harley, P., Wiedinmyer, C., Palmer, P. I., and Geron, C.: Estimates of global terrestrial isoprene emissions using MEGAN (Model of Emissions of Gases and Aerosols from Nature), *Atmos Chem Phys*, 6, 3181-3210, <https://doi.org/10.5194/acp-6-3181-2006>, 2006.
- Guenther, A. B., Jiang, X., Heald, C. L., Sakulyanontvittaya, T., Duhl, T., Emmons, L. K., and Wang, X.: The Model of Emissions of Gases and Aerosols from Nature version 2.1 (MEGAN2.1): an extended and updated framework for modeling biogenic emissions, *Geosci Model Dev*, 5, 1471-1492, <https://doi.org/10.5194/gmd-5-1471-2012>, 2012.
- 610 Guo, S. J., Feng, Y. Y., Wang, L., Dai, M. H., Liu, Z. L., Bai, Y., and Sun, J.: Seasonal variation in the phytoplankton community of a continental-shelf sea: the East China Sea, *Mar Ecol Prog Ser*, 516, 103-126, <https://doi.org/10.3354/meps10952>, 2014.
- Hackenberg, S. C., Andrews, S. J., Airs, R., Arnold, S. R., Bouman, H. A., Brewin, R. J. W., Chance, R. J., Cummings, D., Dall'Olmo, G., Lewis, A. C., Minaeian, J. K., Reifel, K. M., Small, A., Tarran, G. A., Tilstone, G. H., and Carpenter, L. J.: Potential controls of isoprene in the surface ocean, *Global Biogeochem Cy*, 31, 644-662, <https://doi.org/10.1002/2016gb005531>, 2017.
- 615 Hersbach, H., Bell, B., Berrisford, P., Biavati, G., Horányi, A., Muñoz Sabater, J., Nicolas, J., Peubey, C., Radu, R., Rozum, I., Schepers, D., Simmons, A., Soci, C., Dee, D., Thépaut, J.-N. (2023): ERA5 hourly data on single levels from 1940 to present. Copernicus Climate Change Service (C3S) Climate Data Store (CDS), <https://doi.org/10.24381/cds.adbb2d47>, 2023.
- 620 Kameyama, S., Yoshida, S., Tanimoto, H., Inomata, S., Suzuki, K., and Yoshikawa-Inoue, H.: High-resolution observations of dissolved isoprene in surface seawater in the Southern Ocean during austral summer 2010-2011, *J Oceanogr*, 70, 225-239, <https://doi.org/10.1007/s10872-014-0226-8>, 2014.
- Kim, M. J., Novak, G. A., Zoerb, M. C., Yang, M. X., Blomquist, B. W., Huebert, B. J., Cappa, C. D., and Bertram, T. H.: Air-Sea exchange of biogenic volatile organic compounds and the impact on aerosol particle size distributions, *Geophys Res Lett*, 44, 3887-3896, <https://doi.org/10.1002/2017gl072975>, 2017.
- 625 Li, J. L., Kameyama, S., and Yang, G. P.: In-situ measurement of trace isoprene and dimethyl sulfide in seawater and oceanic atmosphere based on room temperature adsorption-thermal desorption, *Mar Chem*, 222, ARTN 103787 <https://doi.org/10.1016/j.marchem.2020.103787>, 2020.
- 630 Li, J. L., Zhang, H. H., and Yang, G. P.: Distribution and sea-to-air flux of isoprene in the East China Sea and the South Yellow Sea during summer, *Chemosphere*, 178, 291-300, <https://doi.org/10.1016/j.chemosphere.2017.03.037>, 2017.
- Li, J. L., Zhai, X., Zhang, H. H., and Yang, G. P.: Temporal variations in the distribution and sea-to-air flux of marine isoprene in the East China Sea, *Atmos Environ*, 187, 131-143, <https://doi.org/10.1016/j.atmosenv.2018.05.054>, 2018.



- Li, J. L., Zhai, X., Ma, Z., Zhang, H. H., and Yang, G. P.: Spatial distributions and sea-to-air fluxes of non-methane
635 hydrocarbons in the atmosphere and seawater of the Western Pacific Ocean, *Sci Total Environ*, 672, 491-501,
<https://doi.org/10.1016/j.scitotenv.2019.04.019>, 2019.
- Liu, X., Xiao, W. P., Landry, M. R., Chiang, K. P., Wang, L., and Huang, B. Q.: Responses of Phytoplankton Communities to
Environmental Variability in the East China Sea, *Ecosystems*, 19, 832-849, <https://doi.org/10.1007/s10021-016-9970-5>,
2016.
- 640 Luo, G. and Yu, F.: A numerical evaluation of global oceanic emissions of alpha-pinene and isoprene, *Atmos Chem Phys*, 10,
2007-2015, <https://doi.org/10.5194/acp-10-2007-2010>, 2010.
- Matsunaga, S., Mochida, M., Saito, T., and Kawamura, K.: In situ measurement of isoprene in the marine air and surface
seawater from the western North Pacific, *Atmos Environ*, 36, 6051-6057, Pii S1352-2310(02)00657-X
[https://doi.org/10.1016/S1352-2310\(02\)00657-X](https://doi.org/10.1016/S1352-2310(02)00657-X), 2002.
- 645 McGillis, W. R., Edson, J. B., Zappa, C. J., Ware, J. D., McKenna, S. P., Terray, E. A., Hare, J. E., Fairall, C. W., Drennan,
W., Donelan, M., DeGrandpre, M. D., Wanninkhof, R., and Feely, R. A.: Air-sea CO₂ exchange in the equatorial Pacific,
J Geophys Res-Oceans, 109, Artn C08s02 <https://doi.org/10.1029/2003jc002256>, 2004.
- Meskhidze, N., Xu, J., Gantt, B., Zhang, Y., Nenes, A., Ghan, S. J., Liu, X., Easter, R., and Zaveri, R.: Global distribution and
climate forcing of marine organic aerosol: 1. Model improvements and evaluation, *Atmos Chem Phys*, 11, 11689-11705,
650 <https://doi.org/10.5194/acp-11-11689-2011>, 2011.
- Myriokefalitakis, S., Vignati, E., Tsigaridis, K., Papadimas, C., Sciare, J., Mihalopoulos, N., Facchini, M. C., Rinaldi, M.,
Dentener, F. J., Ceburnis, D., Hatzianastasiou, N., O'Dowd, C. D., van Weele, M., and Kanakidou, M.: Global Modeling
of the Oceanic Source of Organic Aerosols, *Adv Meteorol*, 2010, Artn 939171 <https://doi.org/10.1155/2010/939171>, 2010.
- NASA Goddard Space Flight Center, Ocean Ecology Laboratory, Ocean Biology Processing Group. Moderate-resolution
655 Imaging Spectroradiometer (MODIS) Terra Chlorophyll Data; 2022 Reprocessing. NASA OB.DAAC, Greenbelt, MD,
USA. <https://doi.org/10.5067/TERRA/MODIS/L3M/CHL/2022>, 2023.
- NASA Goddard Space Flight Center, Ocean Ecology Laboratory, Ocean Biology Processing Group. Moderate-resolution
Imaging Spectroradiometer (MODIS) Terra Downwelling Diffuse Attenuation Coefficient Data; 2022 Reprocessing.
NASA OB.DAAC, Greenbelt, MD, USA. <https://doi.org/10.5067/TERRA/MODIS/L3M/KD/2022>, 2023.
- 660 Novak, G. A. and Bertram, T. H.: Reactive VOC Production from Photochemical and Heterogeneous Reactions Occurring at
the Air-Ocean Interface, *Accounts Chem Res*, 53, 1014-1023, <https://doi.org/10.1021/acs.accounts.0c00095>, 2020.
- Ooki, A., Nomura, D., Nishino, S., Kikuchi, T., and Yokouchi, Y.: A global-scale map of isoprene and volatile organic iodine
in surface seawater of the Arctic, Northwest Pacific, Indian, and Southern Oceans, *J Geophys Res-Oceans*, 120, 4108-
4128, <https://doi.org/10.1002/2014jc010519>, 2015.
- 665 Palmer, P. I. and Shaw, S. L.: Quantifying global marine isoprene fluxes using MODIS chlorophyll observations, *Geophys
Res Lett*, 32, <https://doi.org/10.1029/2005gl022592>, 2005.



- Phillips, D. P., Hopkins, F. E., Bell, T. G., Liss, P. S., Nightingale, P. D., Reeves, C. E., Wohl, C., and Yang, M. X.: Air-sea exchange of acetone, acetaldehyde, DMS and isoprene at a UK coastal site, *Atmos Chem Phys*, 21, 10111-10132, <https://doi.org/10.5194/acp-21-10111-2021>, 2021.
- 670 Rosenfeld, D., Andreae, M. O., Asmi, A., Chin, M., de Leeuw, G., Donovan, D. P., Kahn, R., Kinne, S., Kivekas, N., Kulmala, M., Lau, W., Schmidt, K. S., Suni, T., Wagner, T., Wild, M., and Quaas, J.: Global observations of aerosol-cloud-precipitation-climate interactions, *Rev Geophys*, 52, 750-808, <https://doi.org/10.1002/2013RG000441>, 2014.
- Sabbaghzadeh, B., Upstill-Goddard, R. C., Beale, R., Pereira, R., and Nightingale, P. D.: The Atlantic Ocean surface microlayer from 50 degrees N to 50 degrees S is ubiquitously enriched in surfactants at wind speeds up to 13ms(-1),
675 *Geophys Res Lett*, 44, 2852-2858, <https://doi.org/10.1002/2017gl072988>, 2017.
- Shaw, S. L., Chisholm, S. W., and Prinn, R. G.: Isoprene production by *Prochlorococcus*, a marine cyanobacterium, and other phytoplankton, *Mar Chem*, 80, 227-245, Pii S0304-4203(02)00101-9 [https://doi.org/10.1016/S0304-4203\(02\)00101-9](https://doi.org/10.1016/S0304-4203(02)00101-9), 2003.
- Shaw, S. L., Gantt, B., and Meskhidze, N.: Production and Emissions of Marine Isoprene and Monoterpenes: A Review, *Adv Meteorol*, 2010, Artn 408696 <https://doi.org/10.1155/2010/408696>, 2010.
680
- Simo, R., Cortes-Greus, P., Rodriguez-Ros, P., and Masdeu-Navarro, M.: Substantial loss of isoprene in the surface ocean due to chemical and biological consumption, *Commun Earth Environ*, 3, ARTN 20 <https://doi.org/10.1038/s43247-022-00352-6>, 2022.
- Sinha, V., Williams, J., Meyerhofer, M., Riebesell, U., Paulino, A. I., and Larsen, A.: Air-sea fluxes of methanol, acetone, acetaldehyde, isoprene and DMS from a Norwegian fjord following a phytoplankton bloom in a mesocosm experiment,
685 *Atmos Chem Phys*, 7, 739-755, <https://doi.org/10.5194/acp-7-739-2007>, 2007.
- Tripathi, N., Sahu, L. K., Singh, A., Yadav, R., and Karati, K. K.: High Levels of Isoprene in the Marine Boundary Layer of the Arabian Sea during Spring Inter-Monsoon: Role of Phytoplankton Blooms, *Acs Earth Space Chem*, 4, 583-590, <https://doi.org/10.1021/acsearthspacechem.9b00325>, 2020.
- 690 Uning, R., Latif, M. T., Abd Hamid, H. H., Nadzir, M. S. M., Khan, M. F., and Suratman, S.: Sea-to-Air Fluxes of Isoprene and Monoterpenes in the Coastal Upwelling Region of Peninsular Malaysia, *Acs Earth Space Chem*, 5, 3429-3436, <https://doi.org/10.1021/acsearthspacechem.1c00270>, 2021.
- Wanninkhof, R.: Relationship between wind speed and gas exchange over the ocean revisited, *Limnol Oceanogr-Meth*, 12, 351-362, <https://doi.org/10.4319/lom.2014.12.351>, 2014.
- 695 Wohl, C., Jones, A. E., Sturges, W. T., Nightingale, P. D., Else, B., Butterworth, B. J., and Yang, M. X.: Sea ice concentration impacts dissolved organic gases in the Canadian Arctic, *Biogeosciences*, 19, 1021-1045, <https://doi.org/10.5194/bg-19-1021-2022>, 2022.
- Wohl, C., Li, Q. Y., Cuevas, C. A., Fernandez, R. P., Yang, M. X., Saiz-Lopez, A., and Simo, R.: Marine biogenic emissions of benzene and toluene and their contribution to secondary organic aerosols over the polar oceans, *Sci Adv*, 9, ARTN eadd9031 <https://doi.org/10.1126/sciadv.add9031>, 2023.
700



- Wurl, O., Wurl, E., Miller, L., Johnson, K., and Vagle, S.: Formation and global distribution of sea-surface microlayers, *Biogeosciences*, 8, 121-135, <https://doi.org/10.5194/bg-8-121-2011>, 2011.
- Xu, L., Cameron-Smith, P., Russell, L. M., Ghan, S. J., Liu, Y., Elliott, S., Yang, Y., Lou, S., Lamjiri, M. A., and Manizza, M.: DMS role in ENSO cycle in the tropics, *J Geophys Res-Atmos*, 121, 13537-13558, <https://doi.org/10.1002/2016jd025333>, 2016.
- 705
- Yokouchi, Y., Li, H.-J., Machida, T., Aoki, S., and Akimoto, H.: Isoprene in the marine boundary layer (southeast Asian Sea, eastern Indian Ocean, and Southern Ocean): Comparison with dimethyl sulfide and bromoform, *J. Geophys. Res.*, 104(D7), 8067– 8076, <https://doi.org/10.1029/1998JD100013>, 1999.
- Yu, Z. J. and Li, Y.: Marine volatile organic compounds and their impacts on marine aerosol-A review, *Sci Total Environ*, 710 768, ARTN 145054 <https://doi.org/10.1016/j.scitotenv.2021.145054>, 2021.
- Zhang, W. T. and Gu, D. S.: Geostationary satellite reveals increasing marine isoprene emissions in the center of the equatorial Pacific Ocean, *Npj Clim Atmos Sci*, 5, ARTN 83 <https://doi.org/10.1038/s41612-022-00311-0>, 2022.
- Zhou, L., Booge, D., Zhang, M. M., and Marandino, C. A.: Winter season Southern Ocean distributions of climate-relevant trace gases, *Biogeosciences*, 19, 5021-5040, <https://doi.org/10.5194/bg-19-5021-2022>, 2022.